



ABACO-2: a comprehensive model for microalgae-bacteria consortia validated outdoor at pilot-scale

Rebecca Nordio, Enrique Rodríguez-Miranda, Francesca Casagli, Ana
Sánchez-Zurano, José Luis Guzmán, Gabriel Acién

► To cite this version:

Rebecca Nordio, Enrique Rodríguez-Miranda, Francesca Casagli, Ana Sánchez-Zurano, José Luis Guzmán, et al.. ABACO-2: a comprehensive model for microalgae-bacteria consortia validated outdoor at pilot-scale. *Water Research*, 2024, 248, pp.120837. 10.1016/j.watres.2023.120837 . hal-04397215

HAL Id: hal-04397215

<https://inria.hal.science/hal-04397215>

Submitted on 16 Jan 2024

HAL is a multi-disciplinary open access archive for the deposit and dissemination of scientific research documents, whether they are published or not. The documents may come from teaching and research institutions in France or abroad, or from public or private research centers.

L'archive ouverte pluridisciplinaire **HAL**, est destinée au dépôt et à la diffusion de documents scientifiques de niveau recherche, publiés ou non, émanant des établissements d'enseignement et de recherche français ou étrangers, des laboratoires publics ou privés.



Distributed under a Creative Commons Attribution 4.0 International License

1 **ABACO-2: a comprehensive model for microalgae-bacteria consortia validated outdoor at**
2 **pilot-scale**

3 Rebecca Nordio^{a,b}, Enrique Rodríguez-Miranda^{b,c}, Francesca Casagli^d, Ana Sánchez-Zurano^{a,b},
4 José Luis Guzmán^{b,c}, Gabriel Acién ^{a,b}

5 ^a Department of Chemical Engineering, Universidad de Almería, E04120 Almería, Spain.

6 ^b CIESOL Solar Energy Research Centre, Joint Centre University of Almería-CIEMAT, 04120
7 Almería, Spain.

8 ^c Department of Informatics, Universidad de Almería, E04120 Almería, Spain.

9 ^d Biocore, INRIA centre d'Université Côte d'Azur, Sophia-Antipolis F-06902, France.

10

11 * **Corresponding author:** Rebecca Nordio, rnordio@ual.es

12

13 **Abstract**

14 Modelling microalgae-bacteria in wastewater treatment systems has gained significant attention in
15 the last few years. In this study, we present an enhanced version of the ABACO model, named
16 ABACO-2, which demonstrates improved accuracy through validation in outdoor pilot-scale systems.
17 ABACO-2 enables the comprehensive characterization of microalgae-bacteria consortia dynamics,
18 allowing to predict the biomass concentration (microalgae, heterotrophic bacteria, and nitrifying
19 bacteria) and nutrient evolution. The updated version of the model incorporates new equations for
20 nutrient coefficient yields, oxygen mass balance, and microorganism cellular decay, while
21 significantly reducing the number of calibrated parameters, simplifying the parameter identification.
22 Calibration and validation were performed using data from a 80 m² raceway reactor operated in a
23 semicontinuous mode over an extensive period (May to November, total of 206 days) at a fixed
24 dilution rate of 0.2 day⁻¹ (corresponding to 5 days of hydraulic retention time), where untreated urban
25 wastewater was used as culture medium. ABACO-2 exhibited robustness, accurately forecasting
26 biomass production, population dynamics, nutrient recovery, and prevailing culture conditions across
27 a wide range of environmental and water composition conditions. Mathematical models are essential
28 instruments for the industrial development and optimization of microalgae-related wastewater
29 treatment processes, thereby contributing to the sustainability of the wastewater treatment industry.

30

31

32 **KEYWORDS:** Microalgae, wastewater, modeling

33

34 1. Introduction

35 Water reuse and recycling have become crucial topics of discussion in recent decades, owing to
36 their significant environmental and social implications. With rapid industrialization and population
37 growth, the volume of wastewater generated annually has escalated (Angelakis and Gikas, 2014).
38 contributing to water stress in various regions worldwide, particularly in southern Europe, including
39 Spain, Italy, and Greece (Strosser et al., 2012). Consequently, researchers have directed their efforts
40 toward developing innovative water remediation technologies. Among these technologies,
41 microalgae-based wastewater systems have emerged as a promising solution, capable of replacing
42 traditional secondary and tertiary classical wastewater treatment processes (Abdel-Raouf et al.,
43 2012). The utilization of microalgae in water remediation offers several advantages. Firstly, it
44 demands less energy compared to conventional methods. Secondly, it significantly reduces
45 greenhouse gas emissions. Additionally, microalgae systems eliminate residues effectively and yield
46 valuable biomass, which can be utilized in various industrial applications (Mohd Udaiyappan et al.,
47 2017).

48 Microalgae are photosynthetic microorganisms capable of using CO₂ as a carbon source and light
49 as an energy source, in addition to using nitrogen (N) and phosphorus (P) present in wastewater to
50 produce biomass. Moreover, thanks to the presence of bacteria, the organic matter's degradation is
51 ensured (Muñoz and Guieysse, 2006). The effectiveness of microalgae-based wastewater systems
52 has been demonstrated through pilot-scale testing in raceway reactors (Morillas-España et al.,
53 2021b) and thin layers (Grivalský et al., 2019). These studies have proven that these systems are
54 robust and reliable, enabling the recovery of nutrients from wastewater and producing treated water
55 that meets the regulatory standards set by European legislation (Council Directive of May 1991
56 concerning urban wastewater treatment, 1991). One of the key factors contributing to the success
57 of this technology is its resilience in the face of significant variations in water composition and
58 weather conditions (Nordio et al., 2023). However, high costs and relatively low efficiency are
59 foreclosing the entire industrial development of these systems (Acién et al., 2014). The industrial
60 development of these processes can be possible only after the improved understanding and

61 optimized management of the biological system allowing to study which are the main parameters
62 influencing biomass productivity and the water remediation capacity (Solimeno and García, 2017).

63 In this framework, mathematical modelling serves as a valuable tool for describing these processes;
64 as it enables simulations and performance evaluations under different environmental and process
65 conditions, aiding optimization and the development of control strategies (Solimeno and García,
66 2017). In the literature, it is possible to find many examples of microalgae models that evaluate the
67 growth rate as a function mainly of light, temperature, nutrients and pH (Lee et al., 2015). On the
68 contrary, a few examples of comprehensive models for microalgae-based wastewater treatments
69 are available, defined as models that consider the effect of multiple process parameters and
70 biological mechanisms. Examples of recent comprehensive models are the Zambrano model
71 (Zambrano et al., 2016), the BIOALGAE model (Solimeno et al., 2019), and the ALBA model (Casagli
72 et al., 2021). Nevertheless, it is challenging to obtain validation data over an extended period and
73 using urban wastewater in industrial facilities, so in the literature, some alternatives can be found,
74 such as validations achieved with digestates, synthetic waters, or small-scale reactors. However, it
75 is crucial to develop models that accurately represent the biological system in real conditions (both
76 environmental and operational) since they are intended for use in commercial wastewater treatment
77 facilities. In Spain, for example, there are currently four industrial facilities using microalgae for urban
78 wastewater treatment, employing reactors ranging from 0.5 to 1.0 ha (Masojidek et al., 2022).

79 To apply these models to large-scale production, it is important to balance complexity and realism.
80 For instance, very complex mathematical descriptions of all the metabolic reactions involved in
81 photosynthesis, may not improve the model prediction accuracy, compared to the computational
82 cost required. Additionally, mechanisms that are not relevant for long-time series and continuous
83 conditions can be omitted from the model (Darvehei et al., 2018). Furthermore, in wastewater,
84 thousands of bacterial groups can interact with microalgae, and it is fundamental to carefully select
85 the most relevant groups to reduce the number of equations and the overall complexity. Generally,
86 only a few groups are considered relevant, as they influence nutrient uptake from the culture
87 medium. The first model was proposed by Buhr & Miller in 1983 (Buhr and Miller, 1983), for example,

only two populations (algae and aerobic bacteria) were considered. However, afterwards, the leading bacterial groups identified were the heterotrophic bacteria, which permitted the oxidation of the organic matter, and nitrifying bacteria that compete with microalgae for the consumption of nitrogen (together with phosphorous and carbon) in some cases distinguished between ammonia-oxidizing bacteria (AOB) and nitrite-oxidizing bacteria (NOB) (Aparicio et al., 2022a).

In this work, an improved version of the ABACO model (Sánchez-zurano et al., 2021), named the ABACO-2 model is proposed, calibrated and validated for outdoor conditions. Specifically, new equations are included to reduce the number of calibrated parameters, and the use of the oxygen mass balance allows for improvement in the accuracy of the model. Equations have been implemented using Python language and numpy packages while the calibration has been carried out with Scipy library and the optimization tool that uses the "Nelder-Mead" algorithm. The model has been validated over an extensive period (May-November); data have been collected from a demonstrative pilot-scale raceway reactor of 12 m³ (80 m²) on which the prevailing strain was *Scenedesmus sp.*. The reactor was operated in semi-continuous mode at a fixed rate of 0.2 day⁻¹ using urban wastewater as culture medium. For this study, wastewater not pre-treated besides the removal of large particles was used, so subjected to high variation in terms of composition. This large variability of water nutrient concentration, together with different values of solar radiation and temperature typical of different year seasons, allowed to calibrate and validate the model in a wide range of conditions (Section 2.2), so increasing its prediction accuracy and robustness.

2. Material and methods

2.1. Raceway reactor and inoculum

Experimental data were collected from an 80 m² (12 m³) raceway reactor working in semi-continuous mode between April and December, with a fixed dilution rate of 0.2 day⁻¹. The raceway was installed in the SABANA Demo Plant located in the IFAPA research centre in La Cañada, Almería, Spain. It was composed of a double channel of 40 m and a sump of 0.59 m³ for the gas injections through diffusers and an electric motor connected to a paddlewheel system for culture mixing. The pH was monitored through sensors and controlled through CO₂ injection in the reactor sump. Additionally,

115 an independent airflow allowed reducing the concentration of dissolved oxygen. The culture depth
116 was fixed at 0.15 m. In order to thoroughly monitor the culture dynamics, additional sensors have
117 been installed for recording the dissolved oxygen (0-400% Sat), pH (0-14), temperature (0-80°C)
118 and culture depth (4-40 cm). Moreover, a meteorological station allowed for registering the weather
119 conditions regarding solar radiation and environmental temperature.

120 The chosen inoculum was *Scenedemus sp.* because it was demonstrated to be suitable microalgae
121 that can easily be grown in wastewater and a wide range of conditions (Fernández Sevilla et al.,
122 2006). The strain was initially grown on a fertilizer medium (0.9 g·L⁻¹ of NaNO₃, 0.18 g·L⁻¹ of MgSO₄,
123 0.14 g·L⁻¹ of KH₂PO₄ and 0.003 g·L⁻¹ of Kerantol), first using columns of 0.1 m³ and then in a tubular
124 system of 3 m³ until it reached the concentration of 1 g·L⁻¹. The biomass was then used as inoculum
125 for the raceways. The culture was diluted with wastewater and kept in batch mode for one week,
126 after that being operated in semi-continuous mode until it reached a stable biomass concentration
127 (approximating a steady state condition).

128 **2.2. Environmental conditions and water composition**

129 As previously mentioned, environmental conditions in terms of temperature and radiation were
130 continuously recorded throughout the entire period. The Photosynthetically Active Radiation (PAR)
131 registered were ranged from 2000 μE·m⁻²·s⁻¹ during the months of April and May, gradually
132 decreasing during the colder seasons with peaks at 1200 μE·m⁻²·s⁻¹, with an average of 620 μE·m⁻²·s⁻¹
133 and 350 μE·m⁻²·s⁻¹ respectively. Regarding temperature, the highest values were recorded
134 during the summer season (July-August), reaching peaks of 38°C, while in the spring season (April-
135 May), they ranged between 25-35 °C, and in the autumn season (September-November), between
136 25-12 °C.

137 Regarding the culture medium, it consisted of wastewater collected from the University of Almería
138 during the entire data collection period, except for August when the water was sourced from the
139 primary water treatment plant in the city of Almeria. In both instances, the water underwent pre-
140 treatment, involving the removal of solid particles through an industrial filter (Azud Helix, 200 μm),
141 before being introduced into the culture. During the study period, the nutrient concentration of the

142 wastewater varied over a wide range. Specifically, ammonium (NH_4^+) concentration varies between
143 $10 - 400 \text{ g}\cdot\text{m}^{-3}$, nitrate (NO_3^-) concentration ranged from $0 - 13 \text{ g}\cdot\text{m}^{-3}$, phosphate (PO_4^{2-}) between 30
144 $- 76 \text{ g}\cdot\text{m}^{-3}$, while the chemical oxygen demand (COD) between $100 - 600 \text{ gO}_2\cdot\text{m}^{-3}$.

145 **2.3. Biomass concentration and nutrients analysis**

146 The influent wastewater and the filtered effluent were analysed in terms of nutrient content (N-NO_3^- ,
147 N-NH_4^+ , P-PO_4^{3-}) and COD. The biomass concentration in the culture was daily measured through
148 the dry weight (DW) method. The culture was collected in the morning after the reactor sump, and
149 100 mL were filtered in a $0.5 \mu\text{m}$ filter and let dry for 24h at 80°C in an oven. Regarding the nutrients,
150 they were analysed through colourimetric methodologies in a spectrophotometer according to
151 standard procedures (Standard IC 74246, Standard IC 38364, Standard IC 59755). The total COD
152 was measured with Hanch-Lange kits (LCI-400) and the biodegradable soluble organic matter
153 (BSMO) was estimated as a percentage of the total COD as reported in the literature by Pasztor I.
154 et al., 2009.

155 **2.4. Data collection and analysis**

156 Experimental online data were collected every second by a set of sensors, connected to a
157 Programming Logic Controller (PLC) and a Supervisory Control and Data Acquisition (SCADA)
158 system. On the contrary, data coming from laboratory analysis as described in the previous section,
159 were collected once a day. Given the big amount of data available, it was necessary to perform a
160 prior data analysis following a procedure inspired by the “Cross Industry Standard Process Alliance
161 for Data Mining” (CRISP-DM) approach (Ncr and Clinton, 1999). This methodology is one of the
162 most used among data mining problems and it is composed of six main steps: (i) Business
163 understanding, (ii) Data understanding, (iii) Data preparation, (iv) Modelling, (v) Evaluation, and (vi)
164 Deployment. In this research, the first five steps have been developed as briefly described below:

- 165 I. Business understanding: the objective is to develop a model that can describe the evolution
166 of microalgae-bacteria populations in wastewater-related systems. The aim is to develop a

tool that allows the simulation of the variation of biomass and nutrient concentration with time as a function of environmental and process parameters.

II. Data understanding: data have been collected as described in the previous section, studied, and analysed.

III. Data preparation: Datasets have been ordered, cleaned, and prepared for the modelling step.

IV. Modelling: the biological system has been modelled as described in the next sections. Stepping back to data preparation is often necessary. A part of the experimental data set has been used for the identification of the calibration parameters.

V. Evaluation: the developed model has been validated with long-term outdoor dataset. If the quality of the model was not enough to reach the defined objective, the data preparation and modelling part has been reviewed.

VI. Deployment: this step was not addressed in this research. However, a web interface for model utilization will be developed in future works.

3. Model development

3.1. Model concept

This work considers three microbial groups: microalgae, heterotrophic bacteria and nitrifying bacteria as they are the main actors in the nutrient uptake and the O_2/CO_2 fluxes (Figure 1). During the day, microalgae perform photosynthesis consuming the inorganic carbon and fixing nitrogen and phosphorus while producing O_2 . The preferred nitrogen form for microalgae growth is NH_4^+ , which is highly present in urban wastewater. Microalgae compete with nitrifying bacteria for the uptake of this compound since they use it to transform it into NO_3^- during the nitrification. The nitrification process involved the oxidation of NH_4^+ to NO_2^- by AOB and then NOB transform NO_2^- into NO_3^- . For this study, it is considered that the nitrification is complete because it was not registered a significant concentration of NO_2^- in the culture (consistently below $5\text{ g}\cdot\text{m}^{-3}$). Moreover, microalgae can use NO_3^- as a form of nitrogen, but its consumption takes place only when ammonium is found below a given threshold (prior experimental analysis have estimated it as $80\text{ g}\cdot\text{m}^{-3}$). Heterotrophic bacteria are considered the leading bacteria group as they are the main ones responsible for the degradation of organic matter. For the present work, the COD has been fractionated as proposed by Pasztor I. et

195 al., 2009. Briefly, the total COD can be divided into two main fractions: the biodegradable (readily
196 and slowly) and the non-biodegradable (soluble and particulate). Heterotrophic bacteria can
197 consume only the readily biodegradable organic matter estimated as 22% of the total COD and it
198 will be called BSMO (biodegradable soluble organic matter) in this work. Summarizing, the BSMO
199 concentration is decreased in the culture due to the heterotroph's activity and it can be increased
200 due to the cellular death and decay of the microorganisms present in the culture. Regarding the gas
201 fluxes, the inorganic carbon necessary for microalgae growth is partially provided by the on-demand
202 injection of CO₂ for pH control and the natural release of CO₂ given by bacteria during respiration.
203 This study assumes that microalgae are never limited by inorganic carbon concentration, as CO₂
204 injection always ensures enough carbon availability for microalgal growth, as already demonstrated
205 by previous studies (Posadas et al., 2015). Additionally, experimental data performed into the system
206 indicate that the liquid bulk alkalinity into the medium is never exhausted, preventing the loss of
207 injected CO₂ used for pH control. On the contrary, the O₂ is produced during photosynthesis by
208 microalgae and used by bacteria for their respiration, and it is partially removed from the culture
209 broth due to mass transfer phenomena, mainly aeration into the sump installed on the reactor.

210 ***Main changes implemented from ABACO model***

211 Despite the ABACO model served as the starting point for the development of ABACO-2, significant
212 modifications have been implemented to enhance prediction accuracy and process understanding.
213 Indeed, the ABACO model proposed by Sánchez-zurano et al., 2021, can be considered a
214 preliminary study, conducted with a limited expertise regarding microalgae cultivation phenomena.
215 Furthermore, this model was developed using a restricted dataset and calibrated using data from
216 laboratory-scale experiments conducted under controlled conditions. In contrast, with ABACO-2, the
217 intention is to calibrate parameters under industrial conditions, utilizing a more extensive dataset that
218 encompasses diverse operational and climatic scenarios.

219

220

221 The foremost modification involved the integration of models to account for cell death and respiration,
222 coupled with the variation in BSMO content within the culture, subsequently reduced by heterotrophic
223 bacterial activity. This refinement also led to a reduction in the number of parameters necessitating
224 calibration. As an additional parameter reduction strategy, it was assumed that phosphate
225 consumption by bacteria is minimal and primarily relevant for microalgae. Consequently, phosphate
226 consumption yields for these microorganisms were excluded from the calibration set. Regarding
227 nutrient yields, equations were introduced to describe the dynamics of nutrient uptake by algae as a
228 function of their concentration in the medium. In this context, process rates were adjusted to consider
229 that NO_3 consumption by algae is significant only when NH_4 levels are substantially reduced.
230 Furthermore, in relation to nutrients, a correction parameter was incorporated into the Monod
231 equations to account for nutrient accumulation by microalgae, preventing zero growth in such
232 scenarios. In the context of refining the calibration process, parameters associated with nutrient
233 consumption by bacteria (originally calibrated) were set and adopted from the Activated Sludge
234 Models (ASM), and an oxygen balance was introduced. The O_2 concentration is a continuous
235 measurement within the reactor and it significantly facilitated parameter recognition during the
236 calibration process. Finally, the parameters of the cardinal temperature equations were adjusted
237 using those proposed by Casagli et al., 2021, as they are more representative, having been
238 calibrated while considering winter seasons.

239 **3.2. Model components**

240 This section summarizes the main model components:

- 241 • $S_{\text{NH}_4} [\text{g} \cdot \text{m}^{-3}]$: ammonium. It is present in the influent, and it is consumed especially by microalgae
242 and nitrifying bacteria and in a lower amount by heterotrophic bacteria.
- 243 • $S_{\text{NO}_3} [\text{g}_{\text{NO}_3} \cdot \text{m}^{-3}]$: nitrate. This form of nitrogen is generally null in the influent, but it is generated by
244 the nitrifying bacteria during the nitrification process. Nitrate is consumed by microalgae when
245 ammonium concentration in the medium is low.

- 246 • $S_{PO4} [g_{PO4} \cdot m^{-3}]$: phosphate. Phosphorus is present as a dissolved component in the water inlet.
 247 Its consumption is mainly due to the activity of microalgae, while the uptake from bacteria is
 248 considered negligible.
- 249 • $S_{BSMO} [g_{BSMO} \cdot m^{-3}]$: biodegradable soluble organic matter. This is a fraction of the total COD,
 250 assumed as 22%. It is consumed by heterotrophic bacteria and generated during the cellular
 251 decay of both microalgae and bacteria.
- 252 • $S_{O2} [g_{O2} \cdot m^{-3}]$: dissolved oxygen. Oxygen is produced by microalgae during photosynthesis and
 253 consumed by microalgal respiration and by the activity of both bacterial populations. Moreover,
 254 the dissolved oxygen can be stripped to the atmosphere by bubbling air into the reactor sump.
- 255 • $X_{alg} [g_{alg} \cdot m^{-3}]$: microalgae biomass. Microalgae proliferate starting from an initial inoculum, thus
 256 microalgae biomass is produced by fixing nitrogen and phosphorus, also consuming CO_2 while
 257 producing oxygen. Microalgae concentration in the inlet wastewater is considered negligible,
 258 while a given amount is harvested every day. Moreover, their growth decreases due to cellular
 259 death.
- 260 • $X_{nit} [g_{nit} \cdot m^{-3}]$: nitrifying bacteria biomass. Nitrifying bacteria proliferate starting from an initial
 261 inoculum by consuming nitrogen in the form of ammonium and releasing nitrate. It is assumed
 262 that their concentration entering the system is negligible, while a given concentration is exiting
 263 during the harvesting. Moreover, their growth decreases due to cellular death.
- 264 • $X_{het} [g_{het} \cdot m^{-3}]$: heterotrophic bacteria biomass. Heterotrophic bacteria proliferate starting from an
 265 initial inoculum by consuming the BSMO and nitrogen in the form of ammonium. It is assumed
 266 that their concentration entering the system is negligible, while a given concentration is exiting
 267 during the harvesting. Moreover, their growth decreases due to cellular death.

268 **3.3. Boundary conditions**

269 Concentrations must be always positive or equal to zero. This boundary condition can be expressed
 270 as in equation (1): when a concentration is approaching zero (assuming ε in the order of 10^{-8}), its
 271 derivative has to be equal or more than zero, meaning that it cannot generate negative matters.

$$272 \quad \text{if } X_i \leq \varepsilon \rightarrow \dot{X}_i|_{X_i=0} \geq 0 \quad (1)$$

273 As a result, all the balances implemented for this model have been implemented according to
 274 equation (2), guaranteeing the boundary conditions to be satisfied.

$$275 \quad \dot{X} = f(x, y) \cdot \frac{X}{X + \varepsilon} \quad (2)$$

276 **3.4. Biological processes**

277 Table 1 summarizes the processes taken into consideration of the microalgae and the bacterial
 278 growth, while **Error! Reference source not found.** is the relative matrix of the stoichiometric
 279 parameters. The mass balances for the microorganism's growth have been built according to
 280 equation (3):

$$281 \quad Inlet - Outlet + Reaction = Accumulation \quad (3)$$

282 where the *Inlet* and *Outlet* are the flowrates in [$m^3 \cdot s^{-1}$] in and out of the system, generically defined
 283 as (4) and (5):

$$284 \quad Inlet = Q_d X_{in} \quad (4)$$

$$285 \quad Outlet = Q_h X_{out} \quad (5)$$

286 where Q_d is the dilution flow rate in [$m^3 \cdot s^{-1}$], Q_h is the harvesting flow rate in [$m^3 \cdot s^{-1}$], X_{in}/X_{out} (or S_i/S_{out})
 287 is the concentration of component inlet or outlet in [$g \cdot m^{-3}$].

288 The reaction (r_i , [$g \cdot m^{-3} \cdot day^{-1}$]) term can be obtained by summing the product of the stoichiometric
 289 coefficients, ν_i (Table 3) and the process rate, ρ_j , as described in (6) (Henze et al., 2000)

$$290 \quad r_i = \sum_j \nu_{i,j} \rho_j \quad (6)$$

291 In summary, the processes considered in the ABACO-2 model are:

- 292 • ρ_1 : microalgae growth in NH_4^+ . Microalgae grow photosynthetically using NH_4^+ as a nutrient
 293 source, and contemporarily consuming PO_4^{3+} and CO_2 while producing O_2 .

- 294 • ρ_2 : microalgae growth in NO_3^- . Microalgae grow photosynthetically using NO_3^- as a nutrient
295 source, and contemporarily consuming PO_4^{3+} and CO_2 while producing O_2 . The growth in this
296 nitrogen source is activated only once the medium is decreasing in NH_4^+ concentration.
- 297 • ρ_3 : microalgae decay. This process includes both the algal biomass loss (decay), increasing the
298 BSMO concentration in the medium, and the algal respiration that leads to a consumption of
299 oxygen all over the entire process.
- 300 • ρ_4 : nitrifying bacteria growth. Nitrifying bacteria growth consumes NH_4^+ and O_2 and produces
301 NO_3^- .
- 302 • ρ_5 : nitrifying bacteria decay. Bacterial biomass loss due to their decay; it leads to an increase in
303 the BSMO concentration.
- 304 • ρ_6 : heterotrophic bacteria growth. Heterotrophic bacteria growth consuming the BSMO, O_2 and
305 NH_4^+ .
- 306 • ρ_7 : heterotrophic decay. Bacterial biomass loss due to their decay (it leads to an increase in the
307 BSMO concentration).

308 **3.4.1. Photosynthesis and respiration**

309 The growth rate as a function of light was modelled using the equation proposed by Molina (Grima
310 et al., 1994), as described in equation (7), where I_k in $[\mu\text{E}\cdot\text{m}^{-2}\cdot\text{s}^{-1}]$ is the irradiance constant that
311 represents the equivalent irradiance necessary to reach half of the maximal growth rate, n is the
312 shape constant and I_{av} is the average light inside the reactor in $[\mu\text{E}\cdot\text{m}^{-2}\cdot\text{s}^{-1}]$.

$$313 \quad \mu(I_{av}) = \frac{I_{av}^n}{I_k^n + I_{av}^n} \quad (7)$$

314 The average light inside the culture was expressed following equation (8), and it depends on the
315 incident light I_0 $[\mu\text{E}\cdot\text{m}^{-2}\cdot\text{s}^{-1}]$, the extinction coefficient K_a $[\text{m}^2\cdot\text{g}^{-1}]$, the algal biomass concentration
316 (X_{alg}) in $[\text{g}\cdot\text{m}^{-3}]$ and the culture depth h [m].

$$317 \quad I_{av} = \frac{I_0}{K_a X_{alg} h} (1 - \exp(-K_a X_{alg} h)) \quad (8)$$

Moreover, the average light was used to express the microalgal endogenous respiration as given by equation (9); where m_{max} and m_{min} are the maximum and the minimum respiration in $[\text{day}^{-1}]$, I_{kr} is the irradiance necessary to stop photosynthesis and let begin the respiration and n_r is the shape form for respiration.

$$m_{alg} = m_{min} + \frac{m_{max} I_{av}^{n_r}}{I_{kr}^{n_r} + I_{av}^{n_r}} \quad (9)$$

Finally, bacterial decay has been taken into consideration as a constant effect during the cultivation process. m_{nit} and m_{het} $[\text{day}^{-1}]$ have been modelled as a percentage of the maximum growth rate (as summarized in Table 4) corrected by a coefficient dependent on the temperature θ , as described in equation (10).

$$\theta = \theta_i(T - 20^\circ\text{C}) \quad (10)$$

Where θ_i are specific parameters that depend on the bacterial population considered (Table 3).

3.4.2. Influence of pH, temperature, dissolved oxygen and nutrients

As described in Table 1, for each microorganism, the growth rate depends on a maximum specific growth rate μ value multiplied by a series of normalized factors that depends on the culture conditions of temperature, pH, O_2 and nutrient concentration. The growth rates of microalgae exhibit a bell-shaped function in response to temperature and pH. Initially, as temperature (or pH) increases from low values, the growth rate rapidly increases until it reaches its maximum, corresponding to the optimal parameter value. However, beyond the optimum, the growth rate decreases sharply with further increases in temperature (or pH). The minimum, maximum, and optimal values of these parameters can be determined through laboratory measurements using the photo-respirometric method, and the summarized values are in Table 4. It is possible to observe that bacteria parameters differ from one of the microalgae since their growth is favoured by higher values of both temperature and pH. The growth dependence can be described through a cardinal equation with inflexion, developed for the first time by Bernard et al. (Bernard and Rémond, 2012) (11). Similarly, the model proposed by Ippoliti et al. was used to describe the pH dependence (Ippoliti et al., 2016) (12).

$$\overline{\mu(T)} = \frac{(T - T_{max})(T - T_{min})^2}{(T_{opt} - T_{min})[(T_{opt} - T_{min})(T - T_{opt}) - (T_{opt} - T_{max})(T_{opt} + T_{min} - 2T)]} \quad (11)$$

$$\overline{\mu(pH)} = \frac{(pH - pH_{min})(pH - pH_{max})^2}{(pH_{opt} - pH_{min})[(pH_{opt} - pH_{min})(pH - pH_{opt}) - (pH_{opt} - pH_{max})(pH_{opt} + pH_{min} - 2pH)]} \quad (12)$$

Regarding the effect of dissolved oxygen, it is known that high concentrations are inhibitory for microalgal photosynthesis. According to previous studies on *Scenedemesus sp.*, the growth rate can be reduced by 25% when the concentration is increased up to 150% Sat, while below 250% Sat the photosynthesis is completely stopped. This effect was modelled using the equation proposed by Costache et al., 2013 and reported in equation (13). On the contrary, oxygen has been modelled as a nutrient source for bacteria growth, as described below.

$$\overline{\mu(O_2)_{alg}} = 1 - \left(\frac{S_{O_2}}{S_{O_2,max}} \right)^z \quad (13)$$

Finally, the influence of nutrient concentration on the growth rate was taken into account. As mentioned, nitrogen is a fundamental macronutrient that must be provided to microalgae to ensure their growth. The inorganic nitrogen can be assimilated into acids for the protein formations in many forms, such as NH_4^+ , NO_2^- and NO_3^- . However, in this study, the main nitrogen form present in wastewater was ammonium, while nitrate was formed only after the complete nitrification process. Ammonium is the favoured nitrogen form for microalgae as it requires less energy to be assimilated. Only after a given concentration threshold do microalgae begin to consume NO_3^- , which will be transformed into NH_4^+ to be assimilated into the cells. Phosphate is another fundamental macronutrient for microalgal growth, as it is necessary for the synthesis of RNA into the nucleotides, while it is assumed that this component is not consumed by bacteria. The growth rate as a function of the substrate concentration, has been modelled using the Monod equation, as described in (14), (Monod, 1949)

$$\overline{\mu(S_i)} = \frac{S_i}{S_i + K_s} \quad (14)$$

The Monod equations for the nitrogen and the phosphorus for the process n.1 and 2 in **Error! Reference source not found.** have been modified by the inclusion of a correction factor. With this

modification, zero-growth when no longer nitrogen/phosphate are present in the medium was avoided. Indeed, it is already known that microalgae can store nutrients in cells guaranteeing their survival and growth even when the medium is limited in nutrients. This fact can be represented by more complex models such as the Droop model (Droop, 1970), which considers the cells quota of the limiting element. However, quotas are difficult to be estimated as they required specific laboratory techniques. For this reason, in this work, a simplified description of this phenomenon was chosen by correcting the concentrations in the Monod equation as the sum of the component available in the medium and the one present in the algal biomass (equal to 10% in nitrogen and 2% in phosphorus, multiplied by the “assimilation” factor α) (14), (15).

$$S_N = S_{N,medium} + X_{alg} * 0.1 * \alpha \quad (15)$$

$$S_P = S_{P,medium} + X_{alg} * 0.02 * \alpha \quad (16)$$

The kinetic parameters used for the Monod equation are summarized in Table 3.

3.4.3. Nutrient yields

Nutrient yield can be defined as the amount of nutrients consumed from the medium per gram of biomass produced. In the literature, it can be found that the nutrient yield for algae is not constant, but changes depending on the nutrient amount present in the medium. More specifically, it was found that the nutrient uptake rate is higher at lower nutrient concentrations until it is reached a maximum. This can be explained by some biological mechanisms like the “luxury uptake” (Solovchenko et al., 2019): microalgae store a larger amount of nutrients than the ones necessary for immediate growth. It is possible to suppose that nutrients yield not only depends on the nutrient concentrations in the medium but even on environmental conditions and process parameters. However, modelling this phenomenon is complex, and in the literature can be found different results that mainly depend on the strain used and the type of experiment performed. The equations developed by Zurano et al., 2021 were taken as a good approximation of ammonium and phosphorus consumption rates by microalgae, as described in equation (17), where S is the substrate consumed by microalgae (NH_4^+ , NO_3^- or PO_4^{3-}). It is possible to observe that the equations are the combination of a Monod equation

393 together with a Cardinal limited by a maximum value; the equation parameters are summarized in
 394 Table 5.

$$395 \quad Y_{s,alg} = \left[\frac{Y_{max} S^{ts}}{S_N^{ts} K_{s,Y_s}^{ts}} \right] + \left[\frac{(S - S_{max})(S - S_{min})^2}{(S_{opt} - S_{min}) \left(((S_{opt} - S_{min})(S_N - S_{opt})) - ((S_{opt} - S_{max})(S_{opt} + S_{min} - 2S)) \right)} \right] \quad (17)$$

396 Regarding the nutrient yield of bacteria, the ones proposed by the ASM models (Henze et al.,
 397 2000) were considered a good approximation, and they are summarized in Table 3.

398 **3.4.4. Dissolved oxygen**

399 During the day, microalgae produce oxygen through photosynthesis, which is partially consumed for
 400 algal and bacteria respiration. At the same time, dissolved oxygen can be desorbed to the
 401 atmosphere according to two different phenomena: (i) natural mass transfer from the culture to the
 402 atmosphere in the reactor channels and paddlewheel; (ii) oxygen release and consecutive reduction
 403 of the culture dissolved oxygen thanks to the bubbling of air in the reactor sump. The two phenomena
 404 are represented by two different mass transfer coefficients K_{la} (equal to 1.0 and 110 h⁻¹ respectively)
 405 and Henry law as described in (18):

$$406 \quad m_{O_2} = K_{la_i}(H_{O_2}P_{O_2} - S_{O_2}) \quad (18)$$

407 **4. Model parameters**

408 **4.1. Calibration procedure**

409 Figure 2 represents the calibration strategy adopted. The experimental dataset used to calibrate the
 410 model parameters was selected to include data from different seasons, such as summer, winter, and
 411 intermediate seasons (28/04-15/05, 9/08-15/08, 1/11-15/11). In total, the calibration days chosen
 412 were 41 (20% of the total amount of data). In this way, it was possible to address the parameters by
 413 accounting for various climatic conditions. The final set of parameters was chosen once the objective
 414 function described in (19) was minimized.

$$415 \quad Obj = \sum \frac{\Sigma(y_{sim} - y_{exp})^2}{\sigma_{exp}} \quad (19)$$

where y_{sim} is the model output, y_{exp} the experimental data and σ_{exp} is the experimental data standard deviation. The experimental data used for the model calibration regarded X_{tot} , S_{NH4} , S_{PO4} , S_{NO3} , S_{BSMO} , S_{O2} where X_{tot} was defined as the sum of X_{alg} , X_{nit} and X_{het} and evaluated experimentally as the total dry weight. The model calibration was carried out using Scipy library in Python and “Nelder-Mead” algorithm which is a robust algorithm mainly used for solving unconstrained optimization problems (Gao and Han, 2012). The list of calibrated parameters with their corresponding values is presented in

Table 6.

4.2. Sensitivity analysis

Table 7 presents the findings of a sensitivity analysis that examined all biological and process parameters together with the associated standard deviation. In this analysis, each parameter was individually varied by +/-20% from its nominal value, and the percentage error (20) between the nominal parameter value (y_{nom}) and the varied parameter value (y_{var}) was evaluated.

$$\% \text{ err} = \frac{\sum |y_{nom} - y_{var}|}{\sum y_{var}} * 100 \quad (20)$$

Results indicate that the most sensible parameters are the ones for microalgae growth rate as a function of light (I_{av} , K_a , n), the maximum growth rates of all the organisms ($\mu_{max,alg}$, $\mu_{max,nit}$, $\mu_{max,het}$) and the nutrient yield of NH_4^+ and NO_3^- ($Y_{NH4,alg}$, $Y_{NO3,nit}$, $Y_{NH4,nit}$). Additionally, the cardinal parameters (T_{max} , T_{min} , T_{opt}) of temperature and pH (pH_{max} , pH_{min} , pH_{opt}) show to be highly sensitive. Given their significant impact on the final prediction, these parameters should be carefully selected based on the biological system analysed and the climatic conditions. Notably, only a few of the nutrient yields were deemed relevant to model error.

4.3. Parameters uncertainty and error propagation

Once the most sensible parameters have been identified, it was possible to calculate the model variance and the confidence interval (Denis Dochain, 2001). From the sensitivity analysis, it was

possible to define a sensitivity matrix as (21), which collects the functions of the given output y by varying the parameter p_j .

$$S = \left[\frac{\delta y}{\delta p_1} ; \frac{\delta y}{\delta p_2} ; \dots ; \frac{\delta y}{\delta p_j} \right] \quad (21)$$

The standard deviation of the parameter can be calculated as (22), where C_{jj} is the covariance matrix and p_j is the associated parameter:

$$\vartheta_j^2 = p_j \sqrt{C_{j,j}} \quad (22)$$

The covariance matrix is the inverse of the Fisher information matrix (23), defined as the variance of the score function (Fujita et al., n.d.).

$$F = C^{-1} \quad (23)$$

And it can be calculated starting from the sensitivity analysis according to (24):

$$F = S^T Q^{-1} S \quad (24)$$

where Q is the array of the measured standard deviation.

Once the covariance of the parameter has been evaluated, it was possible to estimate the model error propagation of the output variable y at the given instant time t as (25):

$$\sigma_y(t) = \sqrt{\sum_{i=1}^m S_i(t)^2 \vartheta_{p_j}^2} \quad (25)$$

The model confidence interval at 95% has been calculated on the model output as (26):

$$[y_i - 1.95\sigma_y ; y_i + 1.95\sigma_y] \quad (26)$$

5. Model validation

The model prediction accuracy has been evaluated by calculating the normalized squared root error (NRMSE) and Theil's inequality coefficient (TIC) (H. Theil. et al., 1959), as described in (26), (27). Results are reported in Table 8, it is important to note that when the TIC is lower than 0.3, it is

possible to consider a good agreement between the experimental data and the model predictions. Additionally, Figure 3 to Figure 5 represent the model estimation and the respective experimental data, as described in the next session.

$$NRMSE = \frac{\sqrt{\sum (y_{sim} - y_{exp})^2}}{(y_{exp,max} - y_{exp,min})} \quad (26)$$

$$TIC = \frac{\sqrt{\sum (y_{sim} - y_{exp})^2}}{\sum y_{sim}^2 + \sum y_{exp}^2} \quad (27)$$

Overall, it is possible to affirm that the model can accurately reproduce the biological system. The ABACO-2 model is remarkably accurate for describing the total biomass concentration and the nutrient concentration evolution (NRMSE between 0.14 and 0.23, TIC between 0.16 and 0.24). Additionally, the model accurately can trace the dissolved oxygen in the culture (NRMSE= 0.14, TIC=0.21).

6. Discussion

6.1. Simulation results

Although microalgae-bacteria consortia are considered a promising technology for wastewater treatment, they still address several challenges. An accurate microalgae-bacteria model is a powerful tool to overcome the bottlenecks of this technology (Aparicio et al., 2023). The ABACO-2 model aims to act as a tool for robust and accurate prediction of the evolution of biomass concentration in a microalgae-bacteria system, and, therefore, to differentiate between the evolution of both populations in the face of operational and environmental conditions. Figure 3A represents the evolution of the total biomass concentration from 15th May to 15th November. The dots represent the experimental data while the model is shown with a solid line, and the shading is the model confidence interval at 95%. Total biomass is mean the sum of the contributions of algae and bacteria that can be approximated to the biomass experimentally evaluated through the dry weight method. The results showed that the model reproduces the trend of the experimental data, with a NRMSE=0.21 and TIC=0.16 (Table 8). The concentration of heterotrophic and nitrifying bacteria over the study

485 period is shown in Figure 3B. According to the simulations, heterotrophic bacteria exhibit higher
 486 concentrations than nitrifying bacteria as they vary between 0 and $80 \text{ g}_{\text{het}} \cdot \text{m}^{-3}$, whereas nitrifying
 487 bacteria range from 0 to $10 \text{ g}_{\text{nit}} \cdot \text{m}^{-3}$. Regarding heterotrophic bacteria, the strong fluctuations
 488 observed could be explained by the large variability in the COD concentration in the influent ($100 -$
 489 $600 \text{ gO}_2 \cdot \text{m}^{-3}$). This variability arises from the use of two different types of water sources, one from
 490 the University and the other from the city, with the latter typically containing a higher organic matter
 491 content. The concentration over the months of the nitrifying bacteria was lower, considering their
 492 slower maximum growth rate compared to the one of heterotrophic bacteria. Results show that the
 493 concentration of nitrifying bacteria increased from October to November. This increase may be due
 494 to a reduction in the aeration rate in this specific period, which decreased from $200 \text{ L} \cdot \text{min}^{-1}$ (set-point
 495 in normal operations) to $50 \text{ L} \cdot \text{min}^{-1}$. During that months, the dissolved oxygen concentration
 496 increased in the culture, as the aeration was insufficient to remove it efficiently. Previous studies
 497 have shown that dissolved oxygen concentration strongly influences the growth of microalgae, as it
 498 has an inhibitory effect on photosynthetic activity (Rossi et al., 2020a). Thus, by decreasing the
 499 concentration of microalgae, nitrifying activity is favoured, as both populations compete for the N-
 500 NH_4^+ present in the medium. Previous authors suggested that competition for N-NH_4^+ is the most
 501 frequently negative interaction between microalgae and AOB (Aparicio et al., 2022b). The microalgal
 502 biomass concentration is represented in Figure 3C. Algal productivity is primarily influenced by
 503 variations in light and temperature throughout the seasons (Muñoz and Bernard, 2021). During
 504 spring, the biomass concentration is approximately $0.7 \text{ g}_{\text{alg}} \cdot \text{L}^{-1}$, while in summer it can reach higher
 505 values of up to $1.5 \text{ g}_{\text{alg}} \cdot \text{L}^{-1}$. However, during the colder seasons, it decreases to $0.3 \text{ g}_{\text{alg}} \cdot \text{L}^{-1}$. Overall,
 506 the model effectively captures the evolution of biomass concentration, highlighting the prevalence of
 507 algae biomass compared to bacterial biomass within the culture. Although there is a lack of
 508 experimental data on bacterial concentration, this outcome remains reasonable, supported by
 509 analysis conducted in previous studies on similar systems (Sánchez Zurano et al., 2020).

510 Figure 4 represents the PO_4^{3-} , NO_3^- , NH_4^+ and BSMO concentration in $\text{g} \cdot \text{m}^{-3}$ respectively. In Figure
 511 4A it is shown that the phosphate concentration in the culture can vary between 10 and $60 \text{ g}_{\text{PO}_4} \cdot \text{m}^{-3}$.
 512 The uptake of this component depends only on the activity of microalgae, given that the influence of

bacteria can be considered negligible. In previous studies, it has been demonstrated that the consumption of phosphate is efficient, but not sufficient to lower it to a concentration below the minimum required for the waster discharge (Nordio et al., 2023). Figure 4B represents the NO_3^- concentration, that remained constant from May to October, however, from October to November, it was observed an increase in the NO_3^- concentration, mainly generated during the nitrification process by nitrifiers. The concentration of this compound can vary greatly (between 0 and $300 \text{ g}_{\text{NO}_3} \cdot \text{m}^{-3}$) depending on the activity of the nitrifying bacteria, which, as already explained, was enhanced at the end of the study. Nitrate increase and accumulation in the system can be considered one of the main challenges in microalgae-bacteria-based systems. A decrease in microalgae activity leads to an increase in nitrifying activity, which results in the accumulation of nitrate in the medium. The nitrate generated must be consumed by the microalgae. However, as long as ammonium is available in the medium, it will not be consumed or will be consumed slowly, in breach of discharge regulations. Therefore, ensuring correct microalgae activity is essential to achieve treated water at the end of the process. Regarding the organic matter, its degradation is due to the activity of the heterotrophic bacteria and it can be present with a concentration of up to $250 \text{ g}_{\text{O}_2} \cdot \text{m}^{-3}$ in the culture (Figure 4C). Finally, in Figure 4D there is the evolution of the ammonium concentration. It is possible to observe that, despite the high NH_4^+ concentration entering the system with the wastewater, in the outlet its concentration is mostly lower than $60 \text{ g}_{\text{NH}_4} \cdot \text{m}^{-3}$, meaning that microalgae and nitrifiers can uptake this nutrient with a high efficiency. The peak generated by the simulation is mainly due to the high concentration of this compound entering the system during the dilution/harvesting process at a specific time of the day.

Concluding, Figure 5 represents the simulation of the dissolved oxygen in the culture. Specifically, Figure 5A shows the experimental and simulated values of dissolved oxygen concentration along the entire study period, while Figure 5B shows the representation of the dissolved oxygen concentration in a shorter period. The concentration of dissolved oxygen can reach a high concentration during the day due to the microalgal photosynthesis (up to $25 \text{ mg}_{\text{O}_2} \cdot \text{L}^{-1}$), while it decreases to anoxic conditions during the night due to the couple effect the algae and bacteria respiration.

541 The results obtained show that the evolution of nutrients in the system together with the simulated
542 biomass concentration agree with those obtained in the experimental data, demonstrating the
543 usefulness of ABACO-2 in microalgae-based systems for wastewater treatment, and its potential on
544 an industrial scale.

545 **6.2. Case study: evaluating microalgae-bacteria consortia as function of the operational** 546 **conditions**

547 Studying the populations living in wastewater systems treated with microalgae poses a significant
548 challenge, primarily because there are no fully validated protocols to effectively differentiate between
549 bacterial and microalgal communities. The primary method for assessing biomass in raceway
550 reactors is dry weight, encompassing contributions from both algae and bacteria. Separating them
551 remains challenging yet significant, as their ratios impact various process outcomes, such as
552 biomass quality and water remediation efficiency. Some methods, like successive filtrations based
553 on cell size differences, have been explored, though they often result in a notable presence of
554 bacteria clinging to microalgae due to cell aggregation (Sánchez-Zurano et al., 2020). Alternative
555 methods, including flow cytometry techniques (FCM), prove valuable in assessing the relative
556 composition of mixed microorganism populations, encompassing both prokaryotes and eukaryotes.
557 This approach discriminates between groups by analyzing intrinsic characteristics of individual cells,
558 such as size, complexity, and autofluorescence. Additionally, molecular identification techniques like
559 amplification of 16S and 18S rDNA sequences serve to evaluate microbial community structure
560 (Barreiro-Vescovo et al., 2021). Alongside these methods, photo-respirometry, based on traditional
561 respirometry, has been employed to discern population differences (Rossi et al., 2018). However,
562 these methods lack a direct correlation in biomass concentration ($\text{g}\cdot\text{L}^{-1}$), which is more
563 straightforward to interpret.

564 In this context, mathematical models offer a useful tool of indirectly study how the balance between
565 populations evolves. Operational conditions, notably cultivation height, dilution/harvesting strategy,
566 and oxygen removal capacity, exhibit a substantial influence. This section presents a case study
567 employing the ABACO-2 model to assess how the proportion between algae and bacteria shifts

568 based on the operational conditions. Simulations have been carried out using the same solar
569 radiation and temperature registered for the validation of the model. On the contrary, the inlet values
570 of nutrient concentration have been maintained constant (as a average values measured in the
571 wastewater medium) in order to avoid their influence in the evaluation of the process conditions (180
572 $\text{mg}\cdot\text{L}^{-1} \text{NH}_4^+$, $30 \text{ mg}\cdot\text{L}^{-1} \text{PO}_4^{3-}$, $80 \text{ mg}\cdot\text{L}^{-1} \text{BSMO}$, $3.4 \text{ mg}\cdot\text{L}^{-1} \text{NO}_3^-$).

573 ***Culture height***

574 The cultivation height is one of the fundamental parameters to consider when operating raceway-
575 type reactors as it significantly influences the penetrative capacity of light within the cultivation. It has
576 been demonstrated that light reaches the cells only in the first three centimeters of culture, while the
577 rest remains in a state of darkness due to an effect of autoshading, and, therefore, photosynthetically
578 inactive. Furthermore, light penetration depends on other factors, such as the extinction coefficient
579 (K_a), which can vary from cultivation to cultivation and depends on the property of microalgae to
580 scatter the received light (Barceló-Villalobos et al., 2019).

581 In general, facilities that aim to treat large quantities of water prefer to operate at a rather high culture
582 height, around 30 cm. However, this could be a disadvantage in terms of producing high-quality
583 biomass, as the dark zone favors the growth of bacterial populations over phototrophic ones. Figure
584 6 A,B and C show the populations varying with cultivation height among the seasons (summer,
585 spring and autumn). As expected, at 8 cm, the algal productivity is favored at the expense of the
586 amount of treated water, with the maximum concentration reached in spring as it is the period when
587 the maximum irradiance is reached (Figure 6A). The possibility of being able to increase productivity
588 by reducing the culture height has already been studied through the development of new reactors
589 called "thin layers" that operate at around 2 cm; they have also been tested for treating wastewater
590 in previous studies (Morillas-España et al., 2021a). On the contrary, microalgal concentration
591 decreases as much as the culture height increases, mitigating the effects related to the different
592 seasons, in favour of the proliferation of the bacterial population (Figure 6B,C). This is particularly
593 evident in the case of nitrifiers. An increased water depth and greater availability of ammonium,
594 owing to a reduced uptake capacity by microalgae, enable an increase in their activity. Previous

works demonstrated that the depth of the culture has a striking effect on the composition of the microalgae-bacteria consortia, specially in relative abundance of nitrifiers (Figure 6C). Remarkably, at an 8 cm depth where algae activity is more significant, ammonium consumption mainly occurs within the algae population, resulting in minimal involvement of nitrifying bacteria. Conversely, variations in cultivation height appear to have little effect on the concentration of heterotrophic bacteria (Figure 6B). This is because they do not compete with microalgae for nutrient uptake like nitrifying bacteria; their primary substrate is organic carbon.

In conclusion, the choice of the optimal culture height is of relevance and its regulation mainly depend on the specific goals of the remediation process. These goals may involve achieving high-quality, productive biomass or ensuring efficient water treatment on a larger scale. While a lower culture height is generally recommended to facilitate light penetration, further studies should be carried to avoid heat accumulation and the cellular death. Moreover, it's essential to recognize that significantly increasing the culture depth could enhance the activity of nitrifying bacteria and lead to the accumulation of NO_3^- within the reactor. Based on the outcomes of this simulation study, a culture height of 15 cm appears as a good compromise between treated water quantity, productivity, and balance between algal and bacterial populations.

Dilution/harvesting rate

The harvesting/dilution factor plays a crucial role in microalgae industrial production. When deciding on the best approach to adopt, key considerations include the optimal dilution rate and its application method - whether through continuous or semi-continuous mode. In the first case, dilution occurs gradually over the 12 hours of daylight, while in the latter, both dilution and harvesting take place at specific moments of the day. Figure 6 D, E and F illustrate how varying the dilution rate can impact the productivity and composition of algal-bacterial populations, assuming to operate the reactor in a semi-continuous mode. The optimal dilution rates for algae range between 0.15 to 0.2 day^{-1} , exceeding these rates leads to a significant decrease in productivity (Figure 6D). This finding is consistent with previous research in similar raceway reactors, which suggested a fixed optimal dilution rate of 0.2 day^{-1} throughout the year (Morillas-España et al., 2020). Concerning the bacterial

622 population, it is evident that nitrifying activity decreases significantly beyond a dilution rate of 0.2 day⁻¹. This phenomenon, known as "culture washout," indicates that the growth rate of nitrifying bacteria
623 lags behind the dilution rate, potentially affecting process effectiveness (Figure 6F). Conversely, a
624 contrasting positive impact is observed on heterotrophic bacteria with increased dilution rates (Figure
625 6E). This could be attributed to their rapid growth rate and the enhanced organic matter influx,
626 promoting proliferation.

628 In summary, the simulations presented in this study underscore the critical importance of selecting
629 the optimal dilution factor for the efficient operation of raceway reactors. Traditionally, dilution factors
630 are determined experimentally through batches, which establish the maximum growth rate and
631 consequently the dilution rate. Alternatively, some studies have suggested comparing reactors at
632 different dilutions operated in parallel. While these methods are effective, they can be laborious and
633 time-consuming. Furthermore, conventional laboratory techniques primarily evaluate productivity in
634 terms of dry weight without delving into the dynamics of the populations involved. Therefore, our
635 research demonstrates that a simulation-based approach offers a viable alternative for identifying
636 the most effective dilution and harvesting strategies.

637 ***Air desorption***

638 The concentration of oxygen in a microalgae culture is crucial in biological systems. When oxygen
639 levels surpass air saturation, they can induce inhibitory effects due to the diffusion of dissolved
640 oxygen through microalgae membranes, resulting in oxidative stress on the cells. This inhibitory
641 impact becomes more pronounced with prolonged exposure to elevated oxygen levels (Antonino
642 Baez and Joseph Shiloach, 2014). Microalgae, as photosynthetic organisms, generate oxygen while
643 consuming carbon dioxide, leading to its accumulation in the culture. Studies, such as the one
644 conducted by Rossi et al. in 2020, have shown that excessive oxygen accumulation in cultures can
645 hinder microalgal cell growth (Rossi et al., 2020b). However, there is a scarcity of research assessing
646 how oxygen levels actually influence productivity on a large scale. The prevailing assumption is that
647 oxygen is naturally removed through channels or within the paddlewheel zone. Nonetheless, our

648 experimental data presented herein emphasize the necessity of air injection to reduce oxygen levels
649 in the reactor.

650 Figure 6G, H, and I illustrate the simulation results in scenarios both without air injection and with a
651 K_{La} equal to 110 h^{-1} . Once again, it is evident that forced air input is advantageous in promoting algal
652 population production compared to bacterial populations (Figure 6G). Specifically, when air is not
653 removed, microalgal concentration drastically decreases by 65%, underscoring the significance of
654 air injection in the reactor to lower dissolved oxygen levels. Concerning the bacteria, it's notable that
655 air injection predominantly affects nitrifying population, with heterotrophic ones being less affected.
656 Heterotrophic bacteria exhibit a slight decrease in concentration when air isn't injected. Conversely,
657 nitrifying bacteria show significant growth when oxygen isn't removed from the reactor using
658 compressed air. These results align with the model validation discussed earlier and may offer an
659 explanation for occasional NO_3^- accumulations in cultures. As previously explained, validation data
660 indicated increased nitrification activity when air injection was reduced from 200 L min^{-1} to 50 L min^{-1} ,
661 1 , unfavoring algal growth but favoring nitrification. These simulations confirm this trend, although
662 further experimental studies are needed for confirmation.

663 In conclusion, these simulations reaffirm the critical significance of oxygen removal from the reactor,
664 not only for enhancing productivity but also for ensuring effective water remediation.

665 **Conclusions**

666 ABACO-2 is a comprehensive model for microalgae-bacteria consortia in wastewater systems. The
667 model was calibrated and validated in a pilot-scale wastewater treatment reactor, exposed to
668 environmental changes and fed with real urban wastewater (with daily changes in the concentration
669 of nitrogen, phosphorus and organic matter), over a long period (May-November). The model
670 allowed to predict the biomass, dissolved oxygen and nutrient concentration evolution with high
671 accuracy. Overall, the use of the ABACO-2 model's relative simplicity allows for good predictions
672 while offering advantages in terms of understanding, practicality, efficiency, and versatility.
673 Concluding, the ABACO-2 model can be considered a useful biological model for the description of
674 algae-bacteria in wastewater systems. In order to increase the robustness, in the future it will be

675 necessary to carry out additional validation studies in several data set (accounting for different
676 climatologies and wastewater types) and in higher industrial scales.

677 **Credit authorship contribution statement**

678 **R. Nordio:** Investigation, Formal Analysis, Validation, Software, Data Curation, Visualization, Writing
679 – Original Draft; **E. Rodríguez-Miranda:** Investigation, Formal Analysis, Validation, Software, Data
680 Curation, Writing – Original Draft; **F. Casagli:** Formal analysis, Validation; **A. Sanchez-Zurano:**
681 Investigation, Writing – Original Draft; **J. L. Guzmán:** Conceptualization, Supervision, Writing -
682 Review & Editing, Funding Acquisition; **G. Acien:** Conceptualization, Supervision, Writing - Review
683 & Editing, Funding Acquisition.

684 **Acknowledgements**

685 This research was funded by the H2020 Research and Innovation Programme under the Marie
686 Sklodowska-Curie grant agreement (project: Digitalgaesation, 955520) and by the H2020 Research
687 and Innovation Framework Programme (projects: PRODIGIO, 101007006; REALM, 101060991).
688 Also, this work was supported by the Spanish Ministry of Science and Innovation (project:
689 HYCO2BIO, PID2020-112709RB-C21). All the authors would like to thank the Institute for
690 Agricultural and Fisheries Research and Training (IFAPA).

691 **References**

- 692 Abdel-Raouf, N., Al-Homaidan, A.A., Ibraheem, I.B.M., 2012. Microalgae and wastewater treatment. Saudi J
693 Biol Sci. <https://doi.org/10.1016/j.sjbs.2012.04.005>
- 694 Acien, F.G., Ferná Ndez, J.M., Molina-Grima, E., 2014. Economics of Microalgae Biomass Production.
- 695 Angelakis, A.N., Gikas, P., 2014. Water reuse: Overview of current practices and trends in the world with
696 emphasis on EU states, Water Utility Journal.
- 697 Antonino Baez, Joseph Shiloach, 2014. Effect of elevated oxygen concentration on bacteria, yeasts, and
698 cells propagated for production of biological compounds. Microb Cell Fact 13.
- 699 Aparicio, S., González-Camejo, J., Seco, A., Borrás, L., Robles, Á., Ferrer, J., 2023. Integrated microalgae-
700 bacteria modelling: application to an outdoor membrane photobioreactor (MPBR). Science of the
701 Total Environment 884. <https://doi.org/10.1016/j.scitotenv.2023.163669>
- 702 Aparicio, S., Robles, Á., Ferrer, J., Seco, A., Borrás Falomir, L., 2022a. Assessing and modeling nitrite
703 inhibition in microalgae-bacteria consortia for wastewater treatment by means of photo-

704 respirometric and chlorophyll fluorescence techniques. *Science of the Total Environment* 808.
705 <https://doi.org/10.1016/j.scitotenv.2021.152128>

706 Aparicio, S., Robles, Á., Ferrer, J., Seco, A., Borrás Falomir, L., 2022b. Assessing and modeling nitrite
707 inhibition in microalgae-bacteria consortia for wastewater treatment by means of photo-
708 respirometric and chlorophyll fluorescence techniques. *Science of the Total Environment* 808.
709 <https://doi.org/10.1016/j.scitotenv.2021.152128>

710 Barceló-Villalobos, M., Fernández-del Olmo, P., Guzmán, J.L., Fernández-Sevilla, J.M., Acién Fernández, F.G.,
711 2019. Evaluation of photosynthetic light integration by microalgae in a pilot-scale raceway reactor.
712 *Bioresour Technol* 280, 404–411. <https://doi.org/10.1016/j.biortech.2019.02.032>

713 Barreiro-Vescovo, S., González-Fernández, C., de Godos, I., 2021. Characterization of communities in a
714 microalgae-bacteria system treating domestic wastewater reveals dominance of phototrophic and
715 pigmented bacteria. *Algal Res* 59. <https://doi.org/10.1016/j.algal.2021.102447>

716 Bernard, O., Rémond, B., 2012. Validation of a simple model accounting for light and temperature effect on
717 microalgal growth. *Bioresour Technol* 123, 520–527. <https://doi.org/10.1016/j.biortech.2012.07.022>

718 Buhr, H., O., Miller, S., B., 1983. A dynamic model of the high-rate algal-bacterial wastewater treatment
719 pond. *Water Research* 17, 29–37.

720 Casagli, F., Zuccaro, G., Bernard, O., Steyer, J.P., Ficara, E., 2021. ALBA: A comprehensive growth model to
721 optimize algae-bacteria wastewater treatment in raceway ponds. *Water Res* 190.
722 <https://doi.org/10.1016/j.watres.2020.116734>

723 Costache, T.A., Gabriel Acién Fernandez, F., Morales, M.M., Fernández-Sevilla, J.M., Stamatini, I., Molina, E.,
724 2013. Comprehensive model of microalgae photosynthesis rate as a function of culture conditions in
725 photobioreactors. *Appl Microbiol Biotechnol* 97, 7627–7637. <https://doi.org/10.1007/s00253-013-5035-2>

726

727 Council Directive of May 1991 concerning urban waste water treatment, 1991.

728 Darvehei, P., Bahri, P.A., Moheimani, N.R., 2018. Model development for the growth of microalgae: A
729 review. *Renewable and Sustainable Energy Reviews*. <https://doi.org/10.1016/j.rser.2018.08.027>

730 Denis Dochain, 2001. Bioprocess control , in: Denis Dochain (Ed.), . Wiley-ISTE Series, pp. 52–56.

731 Droop, M.R., 1970. Vitamin B 12 and marine ecology. Continuous culture as an approach to nutritional
732 kinetics. *Journal of the Marine Biological Association of the United Kingdom* 48, 629–636.

733 Fernández Sevilla, J.M., Molina Grima, E., Perez Parra, J., Acién Fernández, F.G., Magán Cañadas, J.J., Friedi,
734 T., 2006. New species of microalgae and its application for animal and human consumption and in the
735 production of carotenoids. WO 2006/087405.

736 Fujita, K., Okada, K., Katahira, K., n.d. The Fisher information matrix: A tutorial for calculation for decision
737 making models.

738 Gao, F., Han, L., 2012. Implementing the Nelder-Mead simplex algorithm with adaptive parameters.
739 *Comput Optim Appl* 51, 259–277. <https://doi.org/10.1007/s10589-010-9329-3>

740 Grima, E.M., Camacho, F.G., Pérez, J.A.S., Sevilla, J.M.F., Fernández, F.G.A., Gómez, A.C., 1994. A
741 mathematical model of microalgal growth in light-limited chemostat culture. *Journal of Chemical*
742 *Technology & Biotechnology* 61, 167–173. <https://doi.org/10.1002/jctb.280610212>

743 Grivalský, T., Ranglová, K., da Câmara Manoel, J.A., Lakatos, G.E., Lhotský, R., Masojídek, J., 2019.
 744 Development of thin-layer cascades for microalgae cultivation: milestones (review). *Folia Microbiol*
 745 (Praha). <https://doi.org/10.1007/s12223-019-00739-7>

746 Henze, Mogens., Gujer, Willi., Mino, Takashi., Van Loosdrecht, Mark., 2000. Activated sludge models ASM1,
 747 ASM2, ASM2d and ASM3. IWA Pub.

748 Ippoliti, D., Gómez, C., del Mar Morales-Amaral, M., Pistocchi, R., Fernández-Sevilla, J.M., Acién, F.G., 2016.
 749 Modeling of photosynthesis and respiration rate for *Isochrysis galbana* (T-Iso) and its influence on the
 750 production of this strain. *Bioresour Technol* 203, 71–79.
 751 <https://doi.org/10.1016/j.biortech.2015.12.050>

752 Lee, E., Jalalizadeh, M., Zhang, Q., 2015. Growth kinetic models for microalgae cultivation: A review. *Algal*
 753 *Res.* <https://doi.org/10.1016/j.algal.2015.10.004>

754 Masojídek, J., Gómez-Serrano, C., Ranglová, K., Cicchi, B., Encinas Bogeat, Á., Câmara Manoel, J.A., Sanches
 755 Zurano, A., Silva Benavides, A.M., Barceló-Villalobos, M., Robles Carnero, V.A., Ördög, V., Gómez
 756 Pinchetti, J.L., Vörös, L., Arbib, Z., Rogalla, F., Torzillo, G., Lopez Figueroa, F., Acién-Fernández, F.G.,
 757 2022. Photosynthesis Monitoring in Microalgae Cultures Grown on Municipal Wastewater as a
 758 Nutrient Source in Large-Scale Outdoor Bioreactors. *Biology (Basel)* 11.
 759 <https://doi.org/10.3390/biology11101380>

760 Mohd Udaiyappan, A.F., Abu Hasan, H., Takriff, M.S., Sheikh Abdullah, S.R., 2017. A review of the
 761 potentials, challenges and current status of microalgae biomass applications in industrial wastewater
 762 treatment. *Journal of Water Process Engineering.* <https://doi.org/10.1016/j.jwpe.2017.09.006>

763 Monod, J., 1949. THE GROWTH OF BACTERIAL CULTURES.

764 Morillas-España, A., Lafarga, T., Acién-Fernández, F.G., Gómez-Serrano, C., González-López, C.V., 2021a.
 765 Annual production of microalgae in wastewater using pilot-scale thin-layer cascade photobioreactors.
 766 *J Appl Phycol* 33, 3861–3871. <https://doi.org/10.1007/s10811-021-02565-2>

767 Morillas-España, A., Lafarga, T., Gómez-Serrano, C., Acién-Fernández, F.G., González-López, C.V., 2020.
 768 Year-long production of *Scenedesmus almeriensis* in pilot-scale raceway and thin-layer cascade
 769 photobioreactors. *Algal Res* 51. <https://doi.org/10.1016/j.algal.2020.102069>

770 Morillas-España, A., Lafarga, T., Sánchez-Zurano, A., Gabriel Acién-Fernández, F., Rodríguez-Miranda, E.,
 771 Gómez-Serrano, C., Cynthia, &, González-López, V., 2021b. Year-long evaluation of microalgae
 772 production in wastewater using pilot-scale raceway photobioreactors: Assessment of biomass
 773 productivity and nutrient recovery capacity.

774 Muñoz, I.L., Bernard, O., 2021. Modeling the influence of temperature, light intensity and oxygen
 775 concentration on microalgal growth rate. *Processes* 9. <https://doi.org/10.3390/pr9030496>

776 Muñoz, R., Guieysse, B., 2006. Algal-bacterial processes for the treatment of hazardous contaminants: A
 777 review. *Water Res.* <https://doi.org/10.1016/j.watres.2006.06.011>

778 Ncr, (, Clinton, J., 1999. CRISP-DM 1.0 Step-by-step data mining guide. DaimlerChrysler.

779 Nordio, R., Delgado, F.J., Sánchez-Zurano, A., Hernandez, J.G., Rodríguez-Miranda, E., Guzmán, J.L., Lafarga,
 780 T., Acién, G., 2023. Long-term assessment of the nutrient recovery capacity and biomass productivity
 781 of *Scenedesmus almeriensis* in raceway reactors using unprocessed urban wastewater. *Bioresour*
 782 *Technol* 369. <https://doi.org/10.1016/j.biortech.2022.128374>

783 Pasztor I., Thury P., Pulai J., 2009. Chemical oxygen demand fractions of municipal wastewater for modeling
784 of wastewater treatment. *International Journal of Environmental Science and Technology* 6, 51–56.

785 Posadas, E., Morales, M. del M., Gomez, C., Ación, F.G., Muñoz, R., 2015. Influence of pH and CO₂ source on
786 the performance of microalgae-based secondary domestic wastewater treatment in outdoors pilot
787 raceways. *Chemical Engineering Journal* 265, 239–248. <https://doi.org/10.1016/j.cej.2014.12.059>

788 Rossi, S., Bellucci, M., Marazzi, F., Mezzanotte, V., Ficara, E., 2018. Activity assessment of microalgal-
789 bacterial consortia based on respirometric tests. *Water Science and Technology* 78, 207–215.
790 <https://doi.org/10.2166/wst.2018.078>

791 Rossi, S., Casagli, F., Mantovani, M., Mezzanotte, V., Ficara, E., 2020a. Selection of photosynthesis and
792 respiration models to assess the effect of environmental conditions on mixed microalgae consortia
793 grown on wastewater. *Bioresour Technol* 305. <https://doi.org/10.1016/j.biortech.2020.122995>

794 Rossi, S., Casagli, F., Mantovani, M., Mezzanotte, V., Ficara, E., 2020b. Selection of photosynthesis and
795 respiration models to assess the effect of environmental conditions on mixed microalgae consortia
796 grown on wastewater. *Bioresour Technol* 305. <https://doi.org/10.1016/j.biortech.2020.122995>

797 Sánchez Zurano, A., Garrido Cárdenas, J.A., Gómez Serrano, C., Morales Amaral, M., Ación-Fernández, F.G.,
798 Fernández Sevilla, J.M., Molina Grima, E., 2020. Year-long assessment of a pilot-scale thin-layer
799 reactor for microalgae wastewater treatment. Variation in the microalgae-bacteria consortium and
800 the impact of environmental conditions. *Algal Res* 50. <https://doi.org/10.1016/j.algal.2020.101983>

801 Sánchez Zurano, A., Gómez Serrano, C., Ación-Fernández, F.G., Fernández-Sevilla, J.M., Molina-Grima, E.,
802 2021. Modeling of photosynthesis and respiration rate for microalgae–bacteria consortia. *Biotechnol*
803 *Bioeng* 118, 952–962. <https://doi.org/10.1002/bit.27625>

804 Sánchez-Zurano, A., Gómez-Serrano, C., Ación-Fernández, F.G., Fernández-Sevilla, J.M., Molina-Grima, E.,
805 2020. A novel photo-respirometry method to characterize consortia in microalgae-related wastewater
806 treatment processes. *Algal Res* 47. <https://doi.org/10.1016/j.algal.2020.101858>

807 Sánchez-zurano, A., Rodríguez-miranda, E., Guzmán, J.L., Ación-fernández, F.G., Fernández-sevilla, J.M.,
808 Grima, E.M., 2021. Abaco: A new model of microalgae-bacteria consortia for biological treatment of
809 wastewaters. *Applied Sciences (Switzerland)* 11, 1–24. <https://doi.org/10.3390/app11030998>

810 Solimeno, A., García, J., 2017. Microalgae-bacteria models evolution: From microalgae steady-state to
811 integrated microalgae-bacteria wastewater treatment models – A comparative review. *Science of the*
812 *Total Environment*. <https://doi.org/10.1016/j.scitotenv.2017.07.114>

813 Solimeno, A., Gómez-Serrano, C., Ación, F.G., 2019. BIO_ALGAE 2: improved model of microalgae and
814 bacteria consortia for wastewater treatment. *Environmental Science and Pollution Research* 26,
815 25855–25868. <https://doi.org/10.1007/s11356-019-05824-5>

816 Solovchenko, A.E., Ismagulova, T.T., Lukyanov, A.A., Vasilieva, S.G., Konyukhov, I. V., Pogosyan, S.I.,
817 Lobakova, E.S., Gorelova, O.A., 2019. Luxury phosphorus uptake in microalgae. *J Appl Phycol*.
818 <https://doi.org/10.1007/s10811-019-01831-8>

819 Strosser, P., Dworak, T., Andrés Garzon Delvaux, P., Berglund, M., Schmidt, G., Mysiak, J., Kossida, M.,
820 Iacovides, I., Ashton, V., Seiz Puyuelo, R., De Paoli, G., Stanley, K., 2012. Gap Analysis of the Water
821 Scarcity and Droughts Policy in the EU Final Report Gap Analysis of the Water Scarcity and Droughts
822 Policy in the EU European Commission.

823 Zambrano, J., Krustok, I., Nehrenheim, E., Carlsson, B., 2016. A simple model for algae-bacteria interaction
824 in photo-bioreactors.

825 Zurano, A.S., Serrano, C.G., Acién-Fernández, F.G., Fernández-Sevilla, J.M., Molina-Grima, E., 2021.
826 Modelling of photosynthesis, respiration, and nutrient yield coefficients in *Scenedemus*
827 *almeriensis* culture as a function of nitrogen and phosphorus. *Appl Microbiol Biotechnol* 105,
828 7487–7503. <https://doi.org/10.1007/s00253-021-11484-8>

829 Tables

830 Table 1.- ABACO-2 model process rates

n.	Process	Process rate [g·m ⁻³ ·day ⁻¹]
1	Microalgae growth on NH ₄	$\mu_{max,alg} \cdot \mu(I_{av}) \cdot \overline{\mu(T)} \cdot \overline{\mu(pH)} \cdot \overline{\mu(O_2)}_{alg} \cdot \overline{\mu(N - NH_4)} \cdot \overline{\mu(P - PO_4)} \cdot X_{alg}$
2	Microalgae growth on NO ₃	$\mu_{max,alg} \cdot \mu(I_{av}) \cdot \overline{\mu(T)} \cdot \overline{\mu(pH)} \cdot \overline{\mu(O_2)}_{alg} \cdot \overline{\mu(N - NO_3)} \cdot \overline{\mu(P - PO_4)} \cdot (1 - \overline{\mu(N - NH_4)}) \cdot X_{alg}$
3	Microalgae decay	$m \cdot X_{alg}$
4	Nitrifying bacteria growth	$\mu_{max,nit} \cdot \overline{\mu_{nit}(T)} \cdot \overline{\mu_{nit}(pH)} \cdot \overline{\mu_{nit}(O_2)} \cdot \overline{\mu_{nit}(N - NH_4)} \cdot X_{nit}$
5	Nitrifying bacteria decay	$\theta_{nit} \cdot m_{nit} \cdot X_{nit}$
6	Heterotrophic bacteria growth	$\mu_{max,het} \cdot \overline{\mu_{het}(T)} \cdot \overline{\mu_{het}(pH)} \cdot \overline{\mu_{het}(O_2)} \cdot \overline{\mu_{het}(N - NH_4)} \cdot \overline{\mu_{het}(BSMO)} \cdot X_{het}$
7	Heterotrophic bacteria decay	$\theta_{het} \cdot m_{het} \cdot X_{het}$

831

832 Table 2.- ABACO-2 stoichiometric matrix

Component	→ i	SNH4	SNO3	SPO4	SBSMO	SO2	Xalg	Xnit	Xhet
j Process ↓		[gNH ₄ ·m ⁻³]	[gNO ₃ ·m ⁻³]	[gPO ₄ ·m ⁻³]	[gBSMO·m ⁻³]	[gO ₂ ·m ⁻³]	[galg·m ⁻³]	[gnit·m ⁻³]	[ghet·m ⁻³]
1 Microalgae growth on NH ₄		$-Y_{NH_4,alg}$		$-Y_{PO_4,alg}$		$+Y_{O_2,alg}$	1		
2 Microalgae growth on NO ₃			$-Y_{NO_3,alg}$	$-Y_{PO_4,alg}$		$+Y_{O_2,alg}$	1		
3 Microalgae endogenous respiration					$1 - f_{alg}$	$-Y_{O_2,alg}$	-1		
4 Nitrifying bacteria growth		$-Y_{NH_4,nit}$	$+Y_{NO_3,nit}$			$-Y_{O_2,nit}$		1	
5 Nitrifying bacteria decay					$1 - f_{bac}$			-1	
6 Heterotrophic bacteria growth		$-Y_{NH_4,het}$			$-Y_{BSMO}$	$-Y_{O_2,het}$			1
7 Heterotrophic bacteria decay					$1 - f_{bac}$				-1

833

834

835

836
837
838
839
840
841
842

Table 3.- Stoichiometric coefficients.

Parameter	Value	Units	Source
$Y_{NH_4,nit}$	7.9	$g_{NH_4} \cdot g_{nit}^{-1}$	(Henze et al., 2000)
$Y_{NO_3,nit}$	26.7	$g_{NO_3} \cdot g_{nit}^{-1}$	(Henze et al., 2000)
$Y_{NH_4,het}$	0.16	$g_{NH_4} \cdot g_{het}^{-1}$	(Henze et al., 2000)
Y_{BSMO}	2.3	$g_{BSMO} \cdot g_{het}^{-1}$	(Henze et al., 2000)
$Y_{O_2,alg}$	1.33	$g_{O_2} \cdot g_{alg}^{-1}$	
$Y_{O_2,nit}$	12.44	$g_{O_2} \cdot g_{nit}^{-1}$	(Henze et al., 2000)
$Y_{O_2,het}$	0.4	$g_{O_2} \cdot g_{het}^{-1}$	(Henze et al., 2000)
f_{alg}	0.1	—	(Solimeno et al., 2019)
f_{bac}	0.1	—	(Solimeno et al., 2019)
θ_{het}	1.07	$^{\circ}C$	(Casagli et al., 2021)
θ_{nit}	1.1	$^{\circ}C$	(Casagli et al., 2021)

843
844

Table 4.- Microalgae kinetic parameters.

Parameter	Value	Units	Source
Microalgae kinetic parameters			
I_K	168	$\mu E \cdot m^{-2} \cdot s^{-1}$	(Sánchez Zurano et al., 2021)
n	1.7	—	(Sánchez Zurano et al., 2021)
K_a	0.08	$m^2 g^{-1}$	This study
I_{K_r}	134	$\mu E \cdot m^{-2} \cdot s^{-1}$	(Sánchez Zurano et al., 2021)
n_r	1.4	—	(Sánchez Zurano et al., 2021)
$T_{min,alg}$	-10	$^{\circ}C$	(Casagli et al., 2021)

$T_{max,alg}$	38	°C	(Casagli et al., 2021)
$T_{opt,alg}$	20	°C	(Casagli et al., 2021)
$pH_{min,alg}$	1.8	—	(Sánchez Zurano et al., 2021)
$pH_{max,alg}$	12.9	—	(Sánchez Zurano et al., 2021)
$pH_{opt,alg}$	8.5	—	(Sánchez Zurano et al., 2021)
$S_{O_2,max}$	22.68	$g_{O_2} \cdot m^{-3}$	(Sánchez Zurano et al., 2021)
z	4.15	—	(Sánchez Zurano et al., 2021)
$K_{S,N-NH_4,alg}$	1.54	$g_{N-NH_4} \cdot m^{-3}$	(Zurano et al., 2021)
$K_{i,N-NH_4,alg}$	571	$g_{N-NH_4} \cdot m^{-3}$	(Zurano et al., 2021)
$n_{N-NH_4,alg}$	2	-	(Zurano et al., 2021)
$K_{S,N-NO_3,alg}$	2.77	$g_{N-NO_3} \cdot m^{-3}$	(Zurano et al., 2021)
$K_{i,N-NO_3,alg}$	387	$g_{N-NO_3} \cdot m^{-3}$	(Zurano et al., 2021)
$n_{N-NO_3,alg}$	2	—	(Zurano et al., 2021)
$K_{S,P-PO_4,alg}$	0.43	$g_{P-PO_4} \cdot m^{-3}$	(Zurano et al., 2021)
Heterotrophic bacteria kinetic parameters			
$T_{min,het}$	-3	°C	(Casagli et al., 2021)
$T_{max,het}$	42	°C	(Casagli et al., 2021)
$T_{opt,het}$	25	°C	(Casagli et al., 2021)
$pH_{min,het}$	6	—	(Sánchez Zurano et al., 2021)
$pH_{max,het}$	12	—	(Sánchez Zurano et al., 2021)
$pH_{opt,het}$	9	—	(Sánchez Zurano et al., 2021)
$K_{S,O_2,het}$	1.98	$g_{O_2} \cdot m^{-3}$	(Sánchez Zurano et al., 2021)
$K_{S,N-NH_4,het}$	0.5	$g_{N-NH_4} \cdot m^{-3}$	(Henze et al., 2000)
$K_{S,BSMO,het}$	0.299	$g_{BSMO} \cdot m^{-3}$	(Henze et al., 2000)
Nitrifying bacteria kinetic parameters			
$T_{min,nit}$	-8	°C	(Casagli et al., 2021)
$T_{max,nit}$	38	°C	(Casagli et al., 2021)

$T_{opt,nit}$	20	$^{\circ}C$	(Casagli et al., 2021)
$pH_{min,nit}$	2	—	(Sánchez Zurano et al., 2021)
$pH_{max,nit}$	13.4	—	(Sánchez Zurano et al., 2021)
$pH_{opt,nit}$	9	—	(Sánchez Zurano et al., 2021)
$K_{s,O_2,nit}$	1.080	$g_{O_2} \cdot m^{-3}$	(Henze et al., 2000)
$K_{s,O_2,nit}$	104.9	$g_{O_2} \cdot m^{-3}$	(Henze et al., 2000)
$K_{S,N-NH_4,nit}$	1	$g_{N-NH_4} \cdot m^{-3}$	(Henze et al., 2000)

846 Table 5.- Microalgae nutrient yield parameters.

Parameter	Value	Units	Source	Parameter	Value	Units	Source	Parameter	Value	Units	Source
$Y_{NH_4,max}$	0.4	$g_{N-NH_4} \cdot g_{alg}^{-1}$	Calibrated	$Y_{NO_3,max}$	0.1	$g_{N-NO_3} \cdot g_{alg}^{-1}$	Calibrated	$Y_{PO_4,max}$	0.003	$g_{P-PO_4} \cdot g_{alg}^{-1}$	Calibrated
K_{S,NH_4}	25	-	(Zurano et al., 2021)	K_{S,NO_3}	25	-	(Zurano et al., 2021)	K_{S,PO_4}	3.2	-	(Zurano et al., 2021)
t_{NH_4}	2	-		t_{NO_3}	2	-		t_{PPO_4}	2.14	-	
$NH_{4,max}$	80	$g_{N-NH_4} \cdot m^{-3}$		$NO_{3,max}$	80	$g_{N-NO_3} \cdot m^{-3}$		$PO_{4,max}$	22	$g_{P-PO_4} \cdot m^{-3}$	
$NH_{4,min}$	10	$g_{N-NH_4} \cdot m^{-3}$		$NO_{3,min}$	10	$g_{N-NO_3} \cdot m^{-3}$		$PO_{4,min}$	2	$g_{P-PO_4} \cdot m^{-3}$	
$NH_{4,opt}$	55	$g_{N-NH_4} \cdot m^{-3}$		$NO_{3,opt}$	55	$g_{N-NO_3} \cdot m^{-3}$		$PO_{4,opt}$	15	$g_{P-PO_4} \cdot m^{-3}$	

847
848
849 Table 6.- List of calibrated parameters and their corresponding values

Parameter	Description	Value	Units
$\mu_{max,alg}$	Maximum algal growth rate	1.5	day^{-1}
m_{min}	Minimum algal respiration rate	0.1	day^{-1}
m_{max}	Maximum algal respiration rate	0.008	day^{-1}
$\mu_{max,nit}$	Maximum nitrifying bacteria growth rate	0.75	day^{-1}
m_{nit}	Nitrifying bacteria decay	$0.05 \mu_{max,nit}$	day^{-1}
$\mu_{max,het}$	Maximum heterotrophic bacteria growth rate	3.4	day^{-1}
m_{het}	Heterotrophic bacteria decay	$0.2 \mu_{max,het}$	day^{-1}
$Y_{NH_4,max}$	NH_4^+ microalage nutrient yield max	0.6	$g_{NH_4} \cdot g_{alg}^{-1}$
$Y_{NO_3,max}$	NO_3^- microalage nutrient yield max	0.1	$g_{NO_3} \cdot g_{alg}^{-1}$
$Y_{PO_4,max}$	PO_4^{3-} microalage nutrient yield max	0.004	$g_{PO_4} \cdot g_{alg}^{-1}$
Kl_a	O_2 natural mass transfer	0.1	h^{-1}
α	Nutrient assimilation coefficient	1	—

851 Table 7.- List of most sensible parameters

Parameter	Units	Nominal value	Standard deviation	Most affected parameters
I_k	$\mu E \cdot m^{-2} \cdot s^{-1}$	168	0.02	$X_{alg}, X_{het}, X_{nit}, S_{NH_4}, S_{NO_3}, S_{PO_4}, S_{BSMO}, S_{O_2}$
K_a	$m^2 g^{-1}$	0.08	1.4E-5	$X_{alg}, X_{het}, X_{nit}, S_{NH_4}, S_{NO_3}, S_{PO_4}, S_{BSMO}, S_{O_2}$
n	—	1.7	1.6E-4	$X_{alg}, X_{het}, X_{nit}, S_{NO_3}, S_{PO_4}, S_{O_2}$
$\mu_{max,alg}$	day^{-1}	1.5	5.38E-4	$X_{alg}, X_{het}, X_{nit}, S_{NH_4}, S_{NO_3}, S_{PO_4}, S_{BSMO}, S_{O_2}$
$\mu_{max,het}$	day^{-1}	3.4	0.0016	X_{het}, S_{BSMO}
$\mu_{max,nit}$	day^{-1}	0.75	0.0004	$X_{nit}, S_{NO_3}, S_{NH_4}$
m_{min}	day^{-1}	0.1	8E-6	$X_{alg}, X_{het}, X_{nit}, S_{NO_3}, S_{BSMO}, S_{O_2}$
m_{nit}	day^{-1}	0.05 $\mu_{max,nit}$	8.34E-5	$X_{het}, X_{nit}, S_{NO_3} S_{BSMO},$
m_{het}	day^{-1}	0.2 $\mu_{max,het}$	6.8E-5	$X_{het}, X_{nit}, S_{NO_3} S_{BSMO},$
$O_{2,max}$	$mg_{O_2} \cdot l^{-1}$	22.68	0.0011	$X_{alg}, X_{het}, X_{nit}, S_{NO_3}, S_{PO_4}, S_{BSMO}, S_{O_2}$
$Y_{NH_4,max}$	—	0.6	0.001	$X_{het}, X_{nit}, S_{NH_4}, S_{NO_3}$
$Y_{NH_4,nit}$	—	0.4	0.016	X_{nit}, S_{NH_4}
$Y_{NO_3,nit}$	—	26.76	0.11	S_{NO_3}
Cardinal parameters	Units	Opt, max, min	Standard deviation	Most affected parameters
T_{alg}	$^{\circ}C$	38,20,-10	0.0026	$X_{alg}, X_{het}, X_{nit}, S_{NH_4}, S_{NO_3}, S_{PO_4}, S_{BSMO}, S_{O_2}$
pH_{alg}	—	8.5, 12.9, 1.8	0.0032	$X_{alg}, X_{het}, X_{nit}, S_{NH_4}, S_{NO_3}, S_{PO_4}, S_{BSMO}, S_{O_2}$
T_{nit}	$^{\circ}C$	20,38,-8	0.04	$X_{het}, X_{nit}, S_{NH_4}, S_{NO_3}, S_{BSMO}$
pH_{nit}	—	9, 13.4, 2	0.024	$X_{het}, X_{nit}, S_{NH_4}, S_{NO_3}, S_{BSMO}$
T_{het}	$^{\circ}C$	25,42,-3	0.034	$X_{het}, X_{nit}, S_{NO_3}, S_{BSMO}$
pH_{het}	—	9, 12, 6	0.0026	$X_{het}, X_{nit}, S_{NO_3}, S_{BSMO}$

852

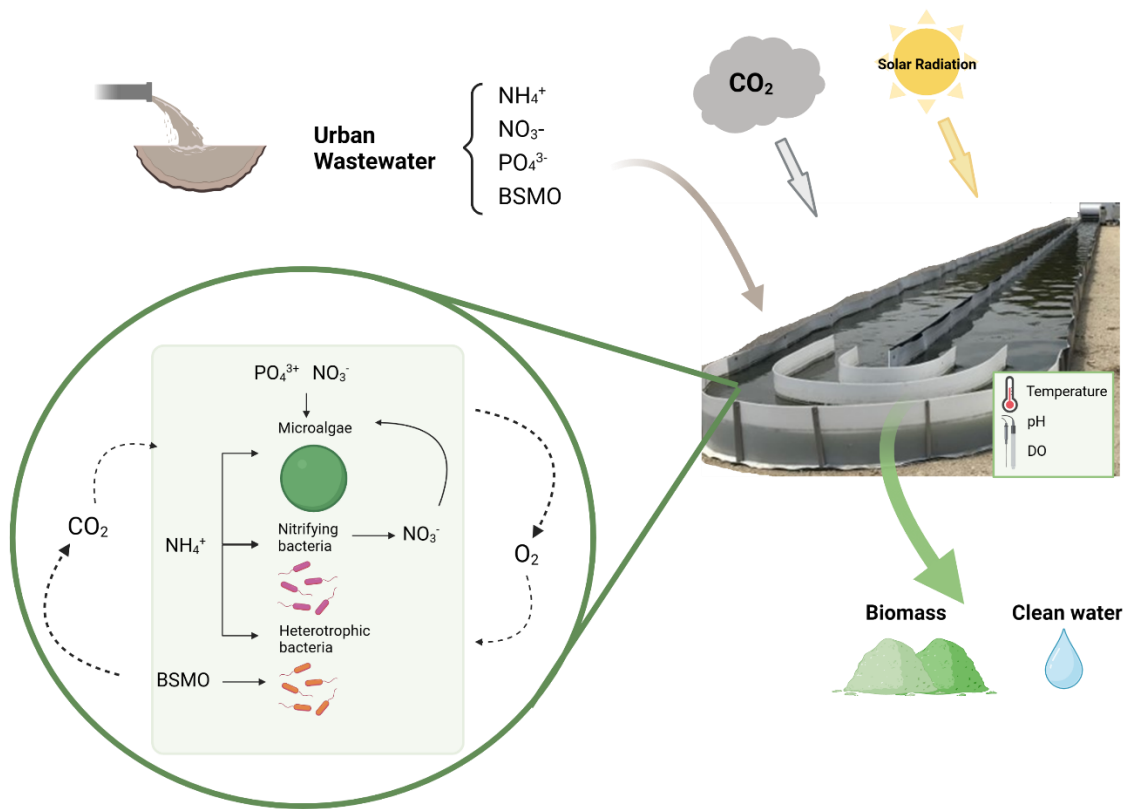
853

854 Table 8.- Validation errors of the ABACO-2 model.

Parameter	NRMSE	TIC
$X_{tot} [g \cdot m^{-3}]$	0.21	0.16
$S_{NH_4} [g \cdot m^{-3}]$	0.22	0.55
$S_{NO_3} [g \cdot m^{-3}]$	0.15	0.21
$S_{PO_4} [g \cdot m^{-3}]$	0.23	0.24
$S_{BSMO} [g \cdot m^{-3}]$	0.21	0.2
$S_{O_2} [g \cdot m^{-3}]$	0.14	0.21

855

856 **Figures**



857

858 Figure 1.- Schematic description of the biological mechanisms taking in place in microalgae-bacteria
859 wastewater systems.

860

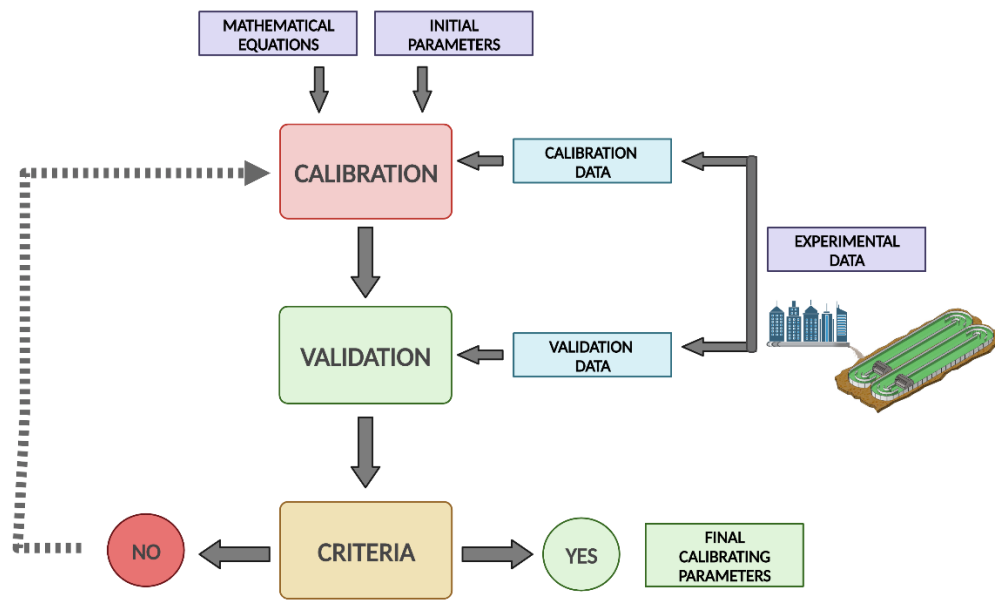


Figure 2.- Calibration methodology used in the present work.

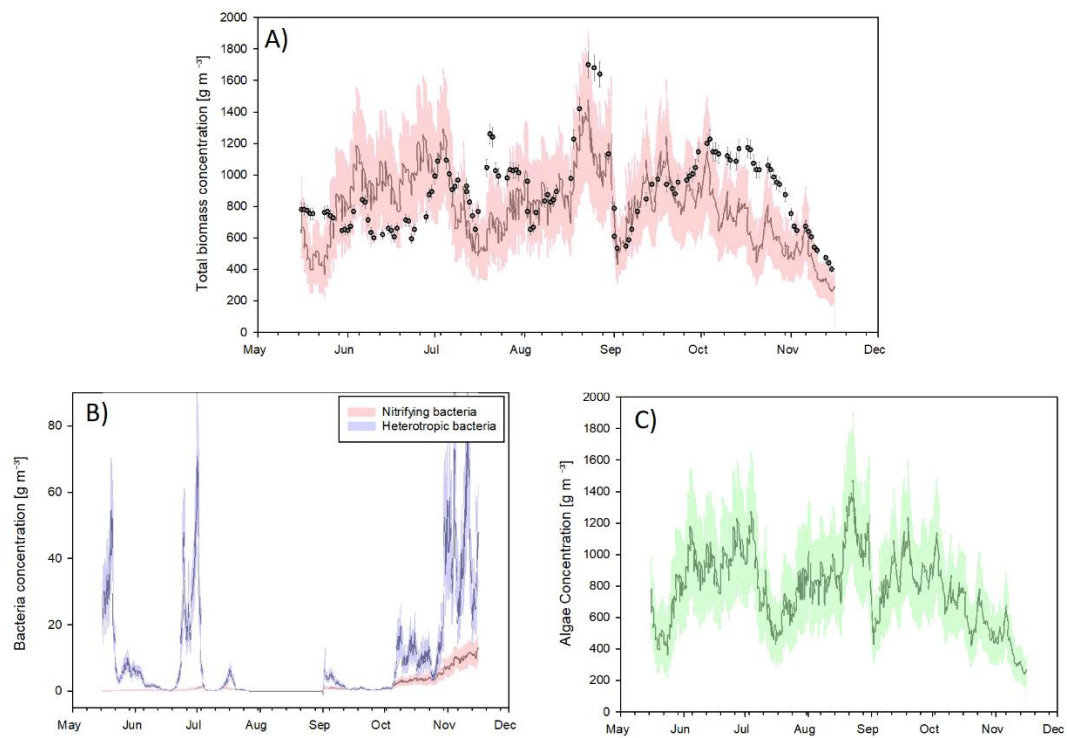
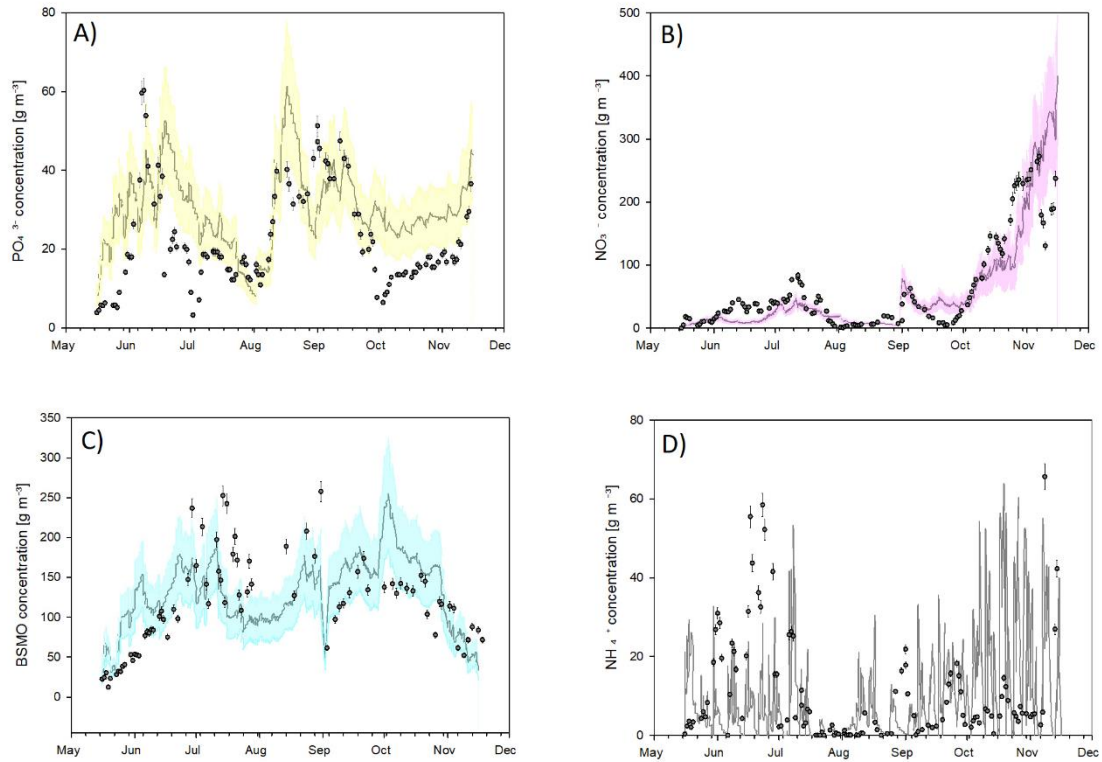


Figure 3.- Biomass concentration evolution. A) Total biomass concentration (sum of algae and bacteria, simulated (continuous line) and experimental (scatter plot); B) Nitrifying and heterotrophic concentration; C) Algae concentration. The model shade is the model confidence interval at 95%.



869

870 Figure 4.- Variation of culture nutrients A) PO_4^{3-} , B) NO_3^- , C) NH_4^+ and D) BSMO concentration, in $\text{g} \cdot \text{m}^{-3}$
 871 respectively (experimental, scatter plot; model prediction, continuous line).

872

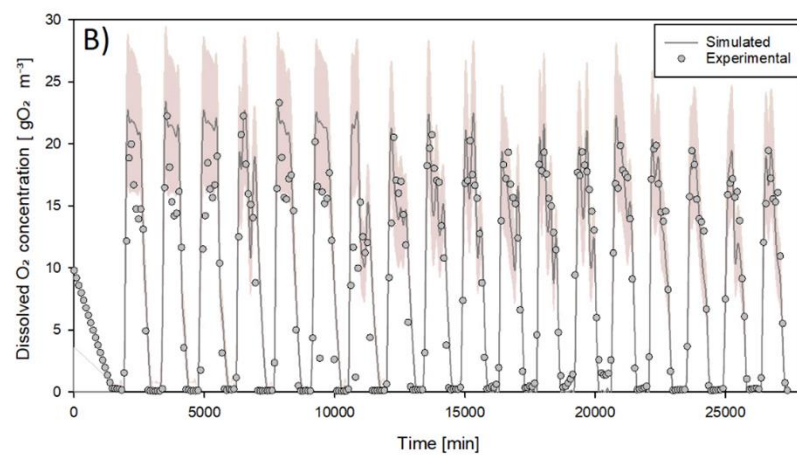
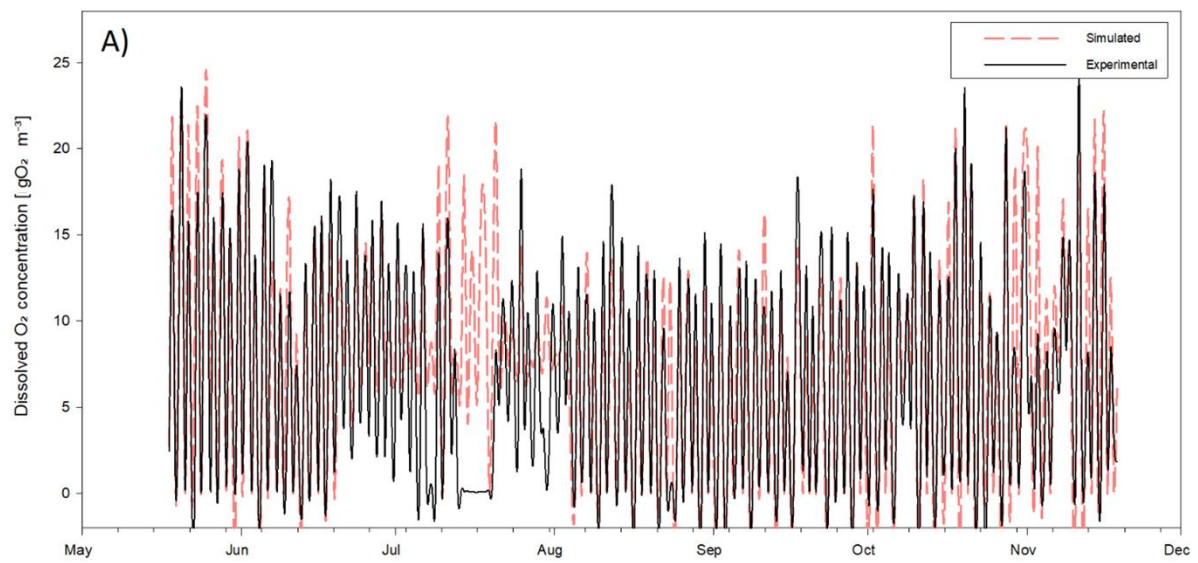
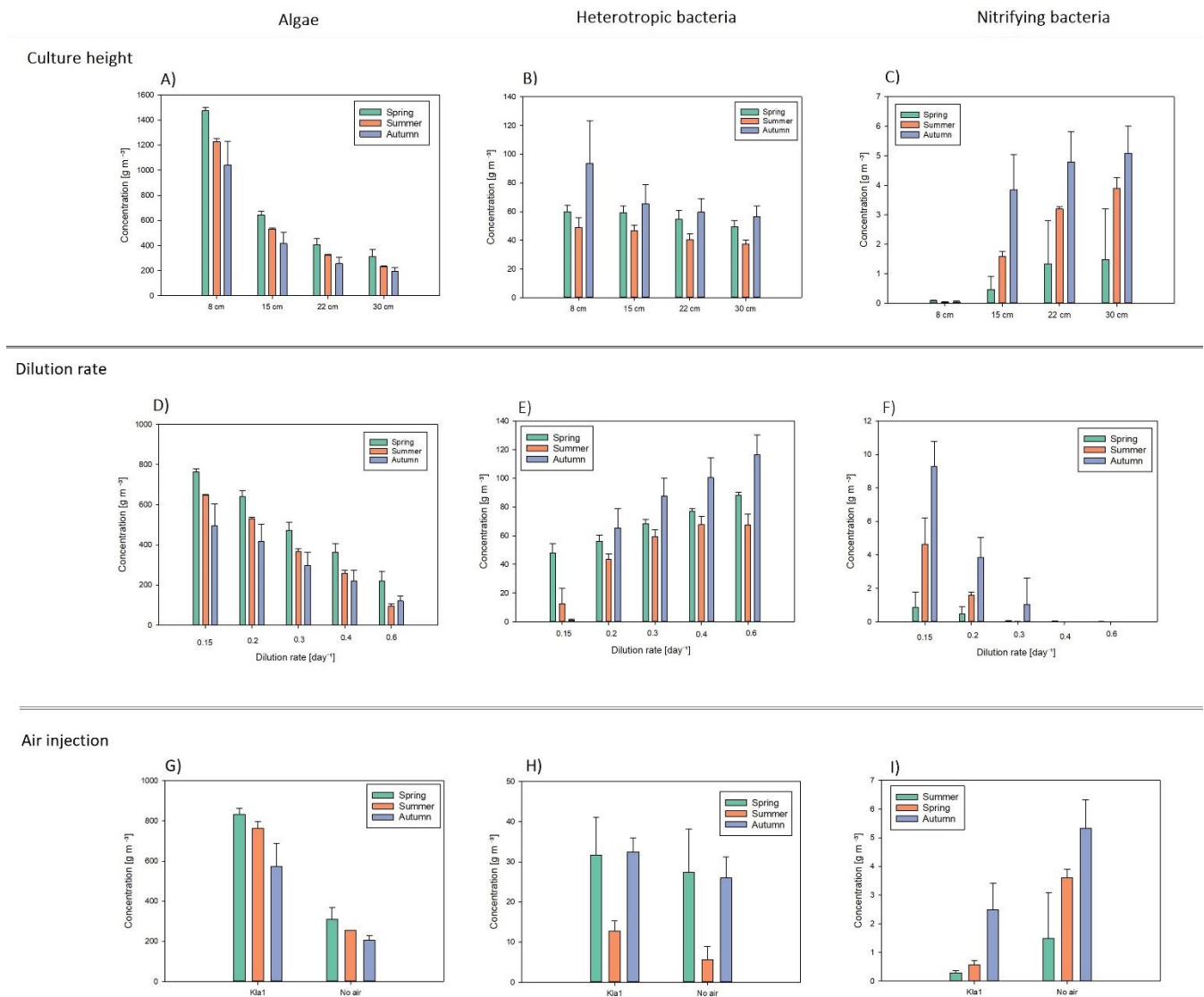


Figure 5.- Simulation of the dissolved oxygen in the culture. A) Experimental and simulated dissolved oxygen along the entire study period, B) Representation of the oxygen in a shorter period.



877

878 Figure 6: Application of ABACO-2 model in a case-study. Algae, heterotrophic and nitrifying bacteria
 879 concentration evolution depending on: A), B), C) culture height; D), E), F) Dilution rate; G), H), I) with or
 880 without injecting air into the system

881

882

